AD-A129 570 STRENGTHENING AND STRENGTH UNIFORMITY OF STRUCTURAL CERAMICS(U) ROCKWELL INTERNATIONAL THOUSAND OAKS CA SCIENCE CENTER F F LANGE MAY 83 SC5295.2AR 1/1

UNCLASSIFIED AFOSR-TR-83-0531 F49620-81-C-0036 F/G 11/2 NL

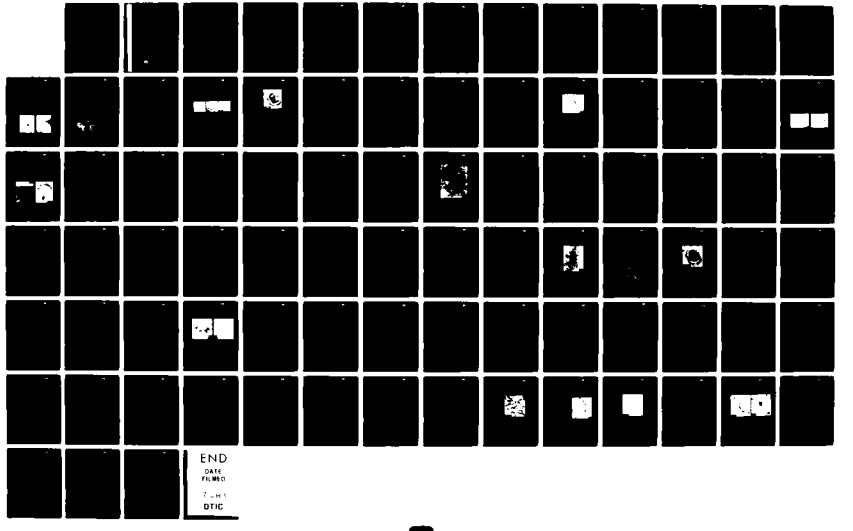

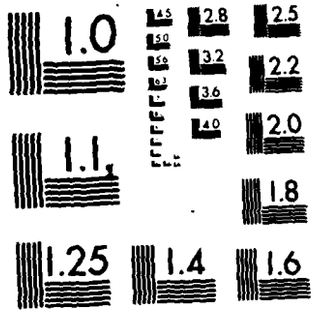

4

SC5295.2AR

Copy No. 4

STRENGTHENING AND STRENGTH UNIFORMITY OF STRUCTURAL CERAMICS

ANNUAL REPORT # 2 FOR THE PERIOD February 1, 1982 through January 31, 1983

CONTRACT NO. F49620-81-C-0036

Prepared for

Air Force Office of Scientific Research
Directorate of Electronic Material Sciences, Bldg. 410
Bolling AFB, DC 20332

F.F. Lange
Principal Investigator

MAY 1983

Rockwell International
Science Center

UNCLASSIFIED

SECURITY CLASSIFICATION OF THIS PAGE (When Data Entered)

REPORT DOCUMENTATION PAGE	READ INSTRUCTIONS BEFORE COMPLETING FORM
1. REPORT NUMBER: AFOSR-TR- 83-0531	2. GOVT ACCESSION NO. / 3. RECIPIENT'S CATALOG NUMBER
4. TITLE (and Subtitle): STRENGTHENING AND STRENGTH UNIFORMITY OF STRUCTURAL CERAMICS	5. TYPE OF REPORT & PERIOD COVERED: Annual Report No. 2 for period 02/01/82 - 01/31/83
	6. PERFORMING ORG. REPORT NUMBER: SC5295.2AR
7. AUTHOR(s): F.F. Lange	8. CONTRACT OR GRANT NUMBER(s): F49620-81-C-0036
9. PERFORMING ORGANIZATION NAME AND ADDRESS: Rockwell International Science Center, 1049 Camino Dos Rios, Thousand Oaks, CA 91360	10. PROGRAM ELEMENT, PROJECT, TASK AREA & WORK UNIT NUMBERS: 2306/A2 61102F
11. CONTROLLING OFFICE NAME AND ADDRESS: Air Force Office of Scientific Research, Directorate of Electronic Material Sciences, Bldg. 410, Bolling AFB, DC 20332	12. REPORT DATE: May 1983
	13. NUMBER OF PAGES: 84
14. MONITORING AGENCY NAME & ADDRESS(if different from Controlling Office)	15. SECURITY CLASS. (of this report): Unclassified
	15a. DECLASSIFICATION/DOWNGRADING SCHEDULE

16. DISTRIBUTION STATEMENT (of this Report)

Approved for public release; distribution unlimited.

17. DISTRIBUTION STATEMENT (of the abstract entered in Block 20, if different from Report)

18. SUPPLEMENTARY NOTES

19. KEY WORDS (Continue on reverse side if necessary and identify by block number)

20. ABSTRACT (Continue on reverse side if necessary and identify by block number)

Stresses created by differential sintering, due to differences in initial bulk density, were determined experimentally. The experiments entailed determining the shrinkage rates of a powder isostatically pressed to two different bulk densities. Using this information, stresses were determined by forcing the slower densifying compact to shrink at the same rate as the faster densifying compact and measuring the resulting forces

DD FORM 1 JAN 73 1473 EDITION OF 1 NOV 65 IS OBSOLETE

UNCLASSIFIED

SECURITY CLASSIFICATION OF THIS PAGE (When Data Entered)

with a load cell. Maximum stresses (between 200 and 400 psi) were observed to occur in the intermediate stage of densification. Despite larger differential strains at higher temperatures, stresses decreased to zero at the latter stage of densification. Viscoelastic experiments, of the stress relaxation type were performed. Results showed that the sintering specimen was more rigid at lower temperatures and more fluid-like at higher temperatures, to explain the development of maximum stresses at intermediate temperatures.

Alumina and Al_2O_3/ZrO_2 (1 to 10 volume%) composite powders were mixed and consolidated by a colloidal method, sintered to >98% theoretical density at 1550°C, and were then subsequently heat treated at temperatures up to 1700°C for grain sizes measurements. Within the temperature range studied, the ZrO_2 inclusions exhibited sufficient self diffusion to move with the Al_2O_3 4-grain junctions during grain growth. Growth of the ZrO_2 inclusions occurred by coalescence. The inclusions exerted a dragging force at the 4-grain junctions to limit grain growth. Abnormal grain growth occurred when the inclusion distribution was not sufficiently uniform to hinder the growth of all Al_2O_3 grains. This condition was observed for compositions containing ≤ 2.5 v/o ZrO_2. Exaggerated grains would consume both neighboring grains and ZrO_2 inclusions. Grain growth control (no abnormal grain grain growth) was achieved when a majority (or all) 4-grain junctions contained a ZrO_2 inclusions, viz for compositions containing ≥ 5 v/o ZrO_2. For this condition the grain size was inversely proportional to the volume fraction of the inclusions. Since the ZrO_2 inclusions mimic voids in all ways except to disappear, it is hypothesized that abnormal grain growth in single phase materials is a result of a nonuniform distribution of voids during the last stage of sintering.

TABLE OF CONTENTS

LIST OF ILLUSTRATIONS

LIST OF ILLUSTRATIONS

LIST OF ILLUSTRATIONS

LIST OF ILLUSTRATIONS

PROGRAM SUMMARY

The goal of this work is to identify the processing flaws that limit the strength of sintered ceramics and to engineer uniform microstructures which either eliminate or minimize the size of these processing flaws. During the first year, a major advance was taken by uncovering the fact that agglomerates in powders produce crack-like voids that severely limit the strength of sintered ceramics (see Appendix I). Crack-like voids produced by the differential sintering of agglomerates relative to their surrounding powder matrix can be the most detrimental strength degrading flaw in sintered ceramics. As detailed and summarized in the review (Appendix I), colloidal approaches to powder processing and consolidation can minimize the size of soft agglomerates (those that can be broken apart with surfactants) and hard agglomerates (eliminated by sedimentation of colloidal suspensions). Work has shown that the elimination of the large soft agglomerates with surfactants increases the average strength of a transformation toughened Al_2O_3/30 v/o ZrO_2 (2.5 v/o Y_2O_3) composite from 550 MPa (80,000 psi) to 930 MPa (135,000 psi). Decreasing the size of the hard agglomerates through sedimentation (supported under Rockwell IR&D) further increases the strength to 1035 MPa (150,000 psi). At this strength level, unusual shaped voids left by organic matter (lint) are observed at fracture origins. During this contract year a new process has been developed to eliminate the void space produced by organic matter which further increases the average strength to 1300 MPa (190,000 psi). One specimen (not included in this average) did not fail after exceeding the load cell limit by 10%. The tensile stress on this specimen exceeded 2000 MPa (300,000 psi). The description of this new process, once confirmed by further testing, will be reported at a later date.

During the current contract year, systematic investigation has concentrated on 1) the stresses that arise during differential shrinkage due to differential initial bulk density (i.e., those stresses that produce the strength degrading crack-like voids) and 2) the control of grain growth with second phases (large grains are fracture origins).

As detailed in Appendix II, the stresses arising due to differential shrinkage were determined experimentally. Results showed (to our surprise) that the maximum stress arises during the early stages of sintering. Stress relaxation experiments showed that despite the lower differential strain and strain rate during the early stage of sintering, the composite was much more elastic, leading to the development of larger stresses. At high temperatures, the relaxation times are very short and thus, stresses can quickly relax to zero. These results have major implications in sintering agglomerated powders, powders with differential compositions (e.g., multi-layered capacitors), and sintered powder/fiber composites by pointing a direction to minimize sintering stresses and eliminating crack-like void formation produced by differential shrinkage.

As detailed in Appendix III, large grains are fracture origins and must be eliminated to increase strength. Use of a second phase (SiC in Al_2O_3) to limit grain growth and increase strength (by 60%) has been demonstrated (Appendix III). Theory shows that despite large residual stresses developed during cooling due to differential thermal contraction, inclusions will not produce strength degrading microcracks if their size is less than a critical size. Thus, inclusions can be incorporated into ceramic microstructures to limit grain size without introducing strength degrading microcracks. The grain growth studies detailed in Appendix IV were carried out with different Al_2O_3/ZrO_2 composites. The principal conclusion of this work was that grain growth control (avoidance of exaggerated grains) could be achieved providing all (or most) of the 4-grain junctions contained an inclusion that hindered grain growth. This condition depends on the size and volume fraction of the inclusion phase, and on the uniformity in which the inclusion phase is distributed. This work has strong implications on engineering the grain size of a material to maximize the potential strength of sintered ceramics.

LIST OF PUBLICATIONS RESULTING FROM CURRENT AFOSR PROGRAMS

1. F.F. Lange, "Processing Related Fracture Origins: Part 1, Observations in Sintered and HIP Treated Al_2O_3/ZrO_2," (in press with J. Am. Ceram. Soc.).

2. F.F. Lange and M. Metcalf, "Processing Related Fracture Origins: Part 2, Agglomerate Motion and Crack-Like Internal Surface Produced by Differential Sintering," (in press with J. Am. Ceram. Soc.).

3. F.F. Lange, I.A. Aksay and B.I. Davis, "Processing Related Fracture Origins: Part 3, Differential Sintering of ZrO_2 Agglomerates in Al_2O_3/ZrO_2 Composites," (in press with J. Am. Ceram. Soc.)

4. F.F. Lange, "Formation of Crack-Like Voids and Agglomerate Motion Due to Differential Sintering," Proc. 5th CIMTEC, (in press).

5. B. Kellett and F.F. Lange, "Stresses Induced by Differential Sintering in Powder Compacts," (to be published).

6. F.F. Lange and Nils Claussen, "Some Processing Requirements for Transformation Toughened Ceramics," Proc. Conf. on Ceramic Ultrastructures, University of Florida, Gainsville, Feb. 1983 (AFOSR-Sponsored) - in press.

7. F.F. Lange and M. Hirlinger, "Hindrance of Grain Growth in Al_2O_3 by ZrO_2 Inclusions," (to be published).

PROGRAM'S CONTRIBUTION TO STUDENT DEVELOPMENT

Two university students were supported under the current AFOSR program:

Mr. Bruce Kellett, a graduate student in the Materials Engineering Department at UCLA, took part in the program to determine the sintering stresses due to differential sintering (see Appendix II). This work is his M.S. thesis topic. He has been accepted to go on for his Ph.D. Dr. F.F. Lange, an Adjunct Professor at UCLA, is his advisor.

Miss Margret Hirlinger, an undergraduate student in the Physics Department at MIT, took part in the grain growth studies (see Appendix IV) during the summer of 1982. She is an outstanding young student who we are encouraging to continue her expertise in Materials Science. She will be working with us again this summer.

APPENDIX I

INFLUENCE OF AGGLOMERATES ON STRENGTH OF SINTERED CERAMICS

INFLUENCE OF AGGLOMERATES ON SINTERED CERAMICS

F.F. Lange
Principal Scientist
Rockwell International Science Center P.O. Box 1085, Thousand Oaks, CA 91360

INTRODUCTION

There are two forms of agglomerates. The first are those which are produced during powder manufacture, e.g., during the decomposition of an oxide precursor. Crystallites produced during decomposition (calcination) partially sinter together to form a hard agglomerate that requires attrition to dismember. Figure 1 illustrates hard agglomerates found in ALCOA 16 Super Ground Al_2O_3 powder which were separated from the fines by sedimentation. This powder contains $\lesssim$ 0.001 volume fraction of these polycrystalline, α-Al_2O_3, hard agglomerates >5 μm. The platy habit of their crystallites (Fig. 1b) strongly suggest

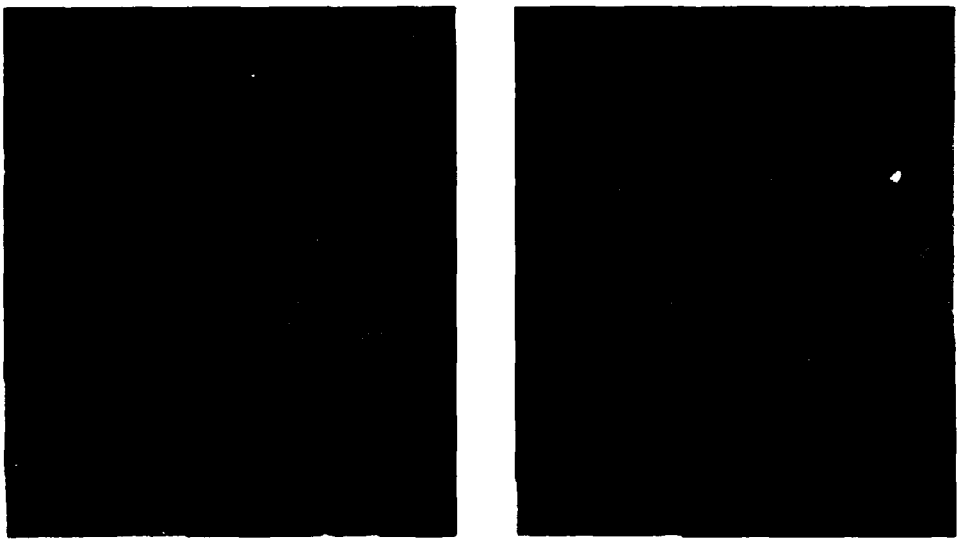

Fig. 1 Hard agglomerate in ALCOA-16SG Al_2O_3 powder.

that they are remnants of the decomposed gibbsite[1] particles not reduced during milling. The second form are soft agglomerates, i.e., those easily broken apart with surfactants (and/or slight mechanical action). Particles in soft agglomerates are held together with either Van der Waals forces or the surface tension of a minor liquid phase. Dry, fine powders used by ceramists usually consist of various sized soft agglomerates (and hard agglomerates), explaining why green densities of <60% theoretical are usually achieved by dry isostatic, pressing whereas large (~50 μm) mono-size spheres, which are unaffected by small particle to particle (e.g., Van der Waals) forces, easily achieve tap densities of ~60%.[2] Figure 2a illustrates the soft agglomerates formed when ALCOA 16SG Al_2O_3 powder (sedimented to 1-5 μm) is dried on a glass slide from a dilute, aqueous suspension for the condition (pH = 9) where interparticle, repulsive forces are minimized. The flocks formed in this suspension settle out on the glass to result in the dried, soft agglomerates shown in Fig. 2a. On the other hand, when the pH of the same suspension is changed to 2.5 by increasing the interparticle repulsion forces in order to allow the particles to settle out and dry in their dispersed state, the rate of flocculation is significantly decreased (Fig. 2b).

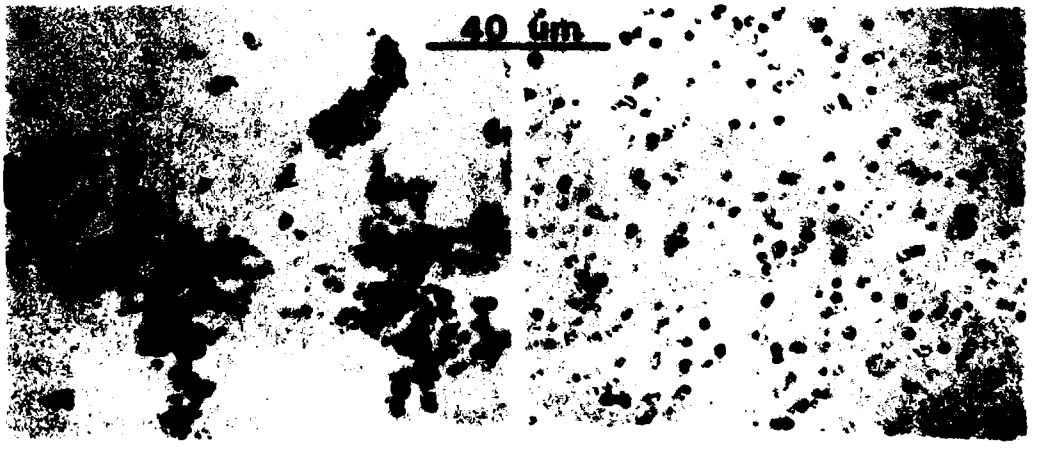

Fig. 2 a) Soft agglomerates formed by flocking ALCOA-16SG Al_2O_3 (1-5 μm) at pH 9. b) Same powder dispersed at pH 2.5.

If one attempts to shake the dried, dispersed particles loose and collect them on another slide, they spontaneously form soft agglomerates similar to those shown in Fig. 1a. One must concede that soft agglomerates are inherent to dry-powder consolidation routes.

The author became interested in agglomerates (and methods of avoiding agglomeration during powder consolidation) when observations suggested that the crack-like voids observed at fracture origins of sintered ceramics were produced by the differential sintering of agglomerates relative to their surrounding powder matrix. It was hypothesized that agglomerates would differ most from one another and from their surrounding powder matrix with respect to green density and that differential sintering was a result of differential green density. To test this hypothesis, large agglomerates were manufactured and incorporated into consolidated powders of differential green density. As reviewed, it was shown that differential sintering due to differential green density not only results in a variety of crack-like voids which can degrade strength, but can also result in agglomerate motion. Further work with Dr. I. Aksay showed that colloidal routes are effective in breaking down soft agglomerates. Consolidation of two phase Al_2O_3/ZrO_2 composites with colloidal routes results in a strength increase of 70% relative to dry powder processing.

CRACK-LIKE VOIDS AT FRACTURE ORIGINS[3]

In an attempt to sinter transformation-toughened Al_2O_3 composites to achieve strengths comparable to those obtained by hot-pressing, a dye-penetrant revealed large (>50 μm), irregular, low density regions on the sectioned surfaces of sintered, dense (>98% TD) materials. It was first hypothesized that these large, low density regions were the strength degrading flaws that limited the strength of the sintered materials to < 1/2 that were obtained by hot-pressing. After experiments involving the hot isostatic pressing (HIP) treatment of sintered materials (which dramatically increased strength) and fractrography, it became evident that the most detrimental flaws were not the low-density regions, but instead were the large internal surfaces which bounded crack-like voids in the sintered materials.

A typical fracture origin for a sintered material, which appears as a slight protrusion, is shown in Fig. 3a. These fracture origins did not absorb the dye penetrant whereas other regions on the fracture surface, remote from the origin, did. Detailed analysis showed that the protrusion's surface had a topograph of a sintered surface as shown in Fig. 3b, whereas the surface remote to the protrusion exhibited a topography typical of a fracture surface as shown in Fig. 3c. These and other observations strongly suggested that the internal surface at the protrusion bounded one-half of a crack-like void.

Fig. 3 a) Protrusion at fracture origin of sintered composite, b) surface topography of protrusion; and c) fracture surface remote from protrusion.

It was hypothesized that the protrusion shown in Fig. 3a was produced by a two phase (Al_2O_3/ZrO_2) agglomerate within the isostatically pressed powder that shrank away from its surrounding powder matrix during sintering to produce a crack-like void responsible for fracture.

More recent experiments have shown that consolidated Al_2O_3/ZrO_2 powders* can also contain single-phase, hard ZrO_2 agglomerates which also produce crack-like voids during sintering. An example of a sectioned ZrO_2 sintered agglomerate and its sectioned crack-like void is shown in Fig. 4.

*Consolidation in this case was carried out by colloidal/filtration (slip casting). The large ZrO_2 hard agglomerates were a result of inefficient ball milling.

SC82-16789

Fig. 4 ZrO_2 agglomerate that shrink away from surrounding Al_2O_3/ZrO_2 matrix during sintering.

DIFFERENTIAL SINTERING OF AGGLOMERATES WITHIN POWDER MATRICES[4]

Effects of differential sintering due to differential green density were studied by fabricating agglomerate powder matrix specimens from two different Al_2O_3 + ZrO_2 (30 volume %) powders and subjecting them to a cyclic sintering schedule to allow intermittent observations. The object of this experimental program was to characterize the phenomena associated with the differential strain developed between the agglomerate and matrix produced by the differential sintering.

Differential Strain

The relation between linear sintering strain (ε), green density (ρ_0) of a powder compact and its density (ρ) at the moment the strain is calculated from specimen dimensions is given by

$$\rho = \frac{\rho_0}{(1-\varepsilon)^3} \quad , \qquad (1)$$

Using Eq. (1) and assuming no interactions, the differential strain ($\Delta\varepsilon = \varepsilon_m - \varepsilon_a$) developed during sintering between an agglomerate (subscript a) and its surrounding matrix (subscript m) can be expressed as

$$\Delta\varepsilon = \left(\frac{\rho_{om}}{\rho_{oa}}\right)^{1/3}\left[\left(\frac{\rho_{oa}}{\rho_{om}}\right)^{1/3}\left(\frac{\rho_a}{\rho_m}\right)^{-1/3} - 1\right] \quad . \tag{2}$$

Equation (2) shows that $\Delta\varepsilon$ is only zero when $\rho_a/\rho_m = \rho_{oa}/\rho_{om}$. Since $\rho_a \to \rho_m \to \rho_t$ (the theoretical density), viz. $\rho_a/\rho_m \to 1$, as sintering proceeds, one can conclude that differential strain will develop during sintering for cases where $\rho_{oa}/\rho_{om} \neq 1$, regardless of the laws governing sintering.

The type of differential strain, i.e., tensile or compressive, will depend on whether the agglomerate densifies faster or slower, respectively, than the matrix and on whether the agglomerate has a higher or lower green density. The magnitude of the stress developed by the differential strain is beyond the scope of the present work.

Specimen Preparation and Observations

Two different Al_2O_3/ZrO_2 composite powders were used. Both contained 30 volume % ZrO_2* (+ 2 mole % Y_2O_3); one was prepared with α-Al_2O_3 (ALCOA 16SG) and the other with γ-Al_2O_3 (Linde B). These composite powders could be sintered to >98% TD by heating to 1600°C for 1 hour.

Cylindrical powder compacts containing a hemispherical surface agglomerate with a green density (different from that of the matrix), were fabricated by the following sequence of operations. Spherical agglomerates (~0.25 cm diameter) were first prepared by cutting an isostatic pressed cylindrical specimen into cubes and abrading the cubes with a high velocity air stream in a cylindrical device layered with SiC paper. High- and low-density agglomerates were made from compacts isostatically pressed at 415 and 70 MPa, respectively. The

*Zircar, Inc. (Monoclinic ZrO_2)

low-density spherical agglomerates were presintered at 1200°C/30 minutes which transformed the γ-Al_2O_3 to α-Al_2O_3 (for the composite powder made with γ-Al_2O_3) and the monoclinic ZrO_2 to tetragonal ZrO_2 (for both powders). The agglomerates were embedded within a cylinderical-shaped matrix powder of the same type. These specimens were then isostatic pressed at 70 to 415 MPa in order to define the green density of the matrix surrounding the agglomerate. The cylindrical specimen was then sanded with SiC paper until the diameter of the agglomerate was intercepted by the sanded surface. This surface was then imprinted with an orthogonal grid (formed on a metal surface) by isostatic pressing (35 MPa). The grid pattern was used to measure the linear sintering strains at the surface and to observe perturbations in the strain pattern around the agglomerate due to differential sintering.

A second route was also developed to produce low-density hemispherical surface agglomerates within a higher density matrix without the need to presinter the agglomerates.

Most agglomerate/matrix specimens were subjected to a sintering schedule which involved successive cyclic heating to a temperature (T = 1200°C, 1300°C, etc.) holding for 15 minutes and then cooling. The sintering strain was determined from displacement of the orthogonal grid pattern with an optical microscope. The agglomerate strain was determined at its center; matrix strain was determined near the periphery of the cylindrical specimen. Specimen dimensions were also used to compute matrix strain and density.

After each sintering cycle, a profilometer trace was made across the specimen, intercepting the center of the agglomerate, to determine surface topography resulting from differential sintering.

After the last sintering cycle, the presence and location of crack-like separations due to differential sintering were determined with a dye penetrant. Subsurface features were also observed by diamond-cutting through the agglomerate.

Effect of Green Density on Densification Rate

The density of one matrix was compared to another at each temperature by plotting their ratio ρ_ℓ/ρ_h as a function of temperature as shown in Fig. 5. This figure shows that ρ_ℓ/ρ_h begins to increase and approaches 1 prior to either compact achieving its end-point density. Also, since ρ_ℓ/ρ_h is always greater than $\rho_{o\ell}/\rho_{oh}$ (the green density ratio of the couple under comparison), one must conclude that the lower density compact (defined by ρ_ℓ) densifies at a greater rate than the higher density compact (defined by ρ_h). This result is in accordance with Bruch's[5] observations for the regime of "normal sintering," viz. compacts with lower green densities initially sinter at a faster rate than do compacts with higher green densities.

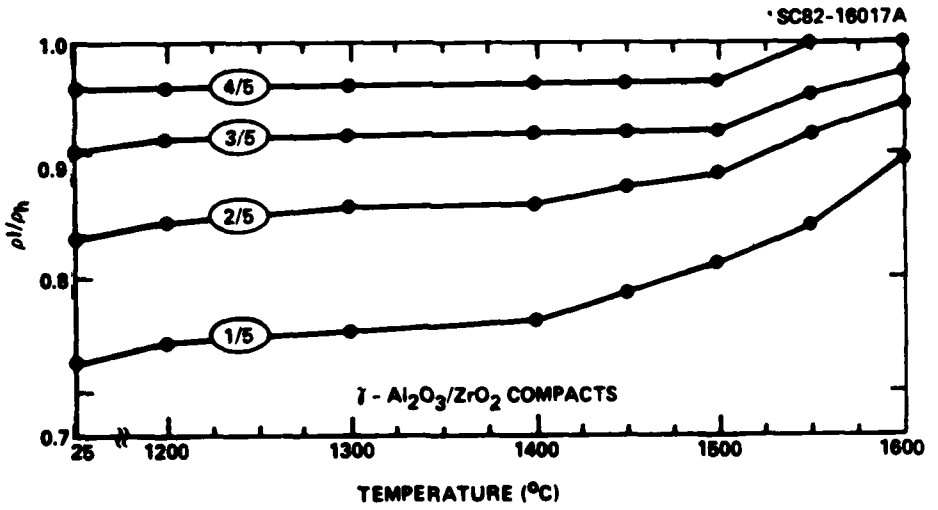

Fig. 5 Density ratio of compact pairs as a function of sintering temperature (4).

Agglomerate/Matrix Densification

Figure 6 illustrates the agglomerate/matrix density ratio (ρ_a/ρ_m) as a function of temperature. For the cases where the green density of the agglomerate was greater than the matrix (Fig. 6a), $\rho_a/\rho_m < \rho_{oa}/\rho_{om}$ and tended toward unity with increasing temperature. That is, the lower density matrix exhibited

a greater densification rate relative to the higher density agglomerate. Comparing these results with Eq. (2) one can see that the matrix always exerts a compressional strain (and stress) on the agglomerate. These results are general for specimens fabricated from both powders.

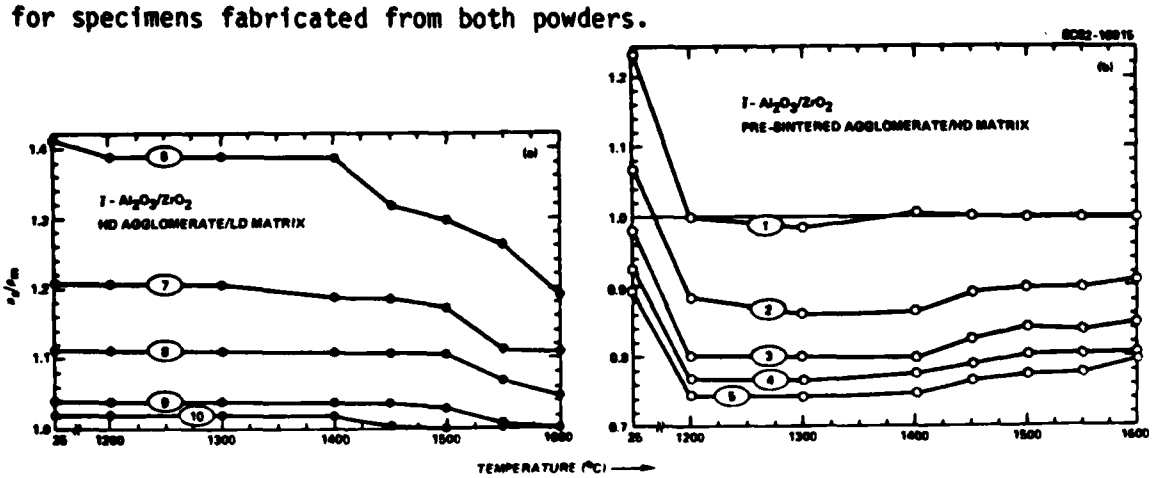

Fig. 6 Agglomerate to matrix density ratio vs sintering temperature for a) higher density agglomerates, and b) presintered agglomerates (4).

For cases where the agglomerates were presintered at 1200°C/30 minutes prior to their insertion into the higher green density matrix, the ρ_a/ρ_m vs temperature relation is more complicated. The large decrease in ρ_a/ρ_m that occurred during the first cycle (heating to 1200°C) was caused by the phase transformations ($\gamma \rightarrow \alpha$-$Al_2O_3$ and m→t-ZrO_2) within the matrix (which produce a linear shrinkage of ~6%) surrounding the agglomerate that had previously undergone the same transformations during presintering (a linear strain of ~0% was recorded for the agglomerate during the first sintering cycle). A similar, but smaller effect was observed for specimens fabricated with the α-Al_2O_3 powder (where, the initial decrease in ρ_a/ρ_m was only produced by the m→t-ZrO_2 transformation). Comparing these results with Eq. (2), it can be seen that during the large, initial decrease in ρ_a/ρ_m, the matrix exerts a large compressive strain on the agglomerate. As sintering proceeds, and as ρ_a/ρ_m increases from its minimum, the compressive strain diminishes. For several specimens (not shown in Fig. 6b), the strain reversed to tension during the latter stages of sintering (when $\rho_a/\rho_m > \rho_{oa}/\rho_{om}$).

Figure 7 illustrates the perturbations in the grid pattern adjacent to the agglomerate produced by differential sintering for the case where ρ_a/ρ_m was persistently less than ρ_{oa}/ρ_{om} during the full sintering schedule.

SC82-15944

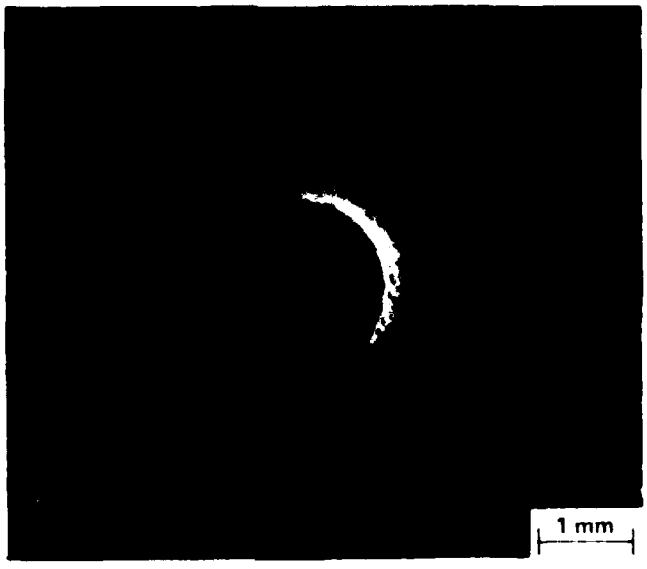

Fig. 7 Perturbations produced in the orthogonal grid pattern by differential sintering. Note agglomerate's protrusion (4).

It was shown that the radial and tangential strains within the matrix can be represented as

$$\varepsilon_r = \varepsilon_m + 2\Delta\varepsilon\,(R/r)^3$$

and

$$\varepsilon_t = \varepsilon_m - \Delta\varepsilon\,(R/r)^3$$

where ε_r is the matrix strain at $R/r \to 0$ (R is the radius of the agglomerate and r is the radius vector parallel to the surface). Thus, for the cases where $\rho_a/\rho_m < \rho_{oa}/\rho_{om}$, the lower densification rate of the agglomerate restricts the tangential sintering strain of the matrix by $\Delta\varepsilon(R/r)^3$ and enhances its radial

sintering strain by $2\Delta\varepsilon(R/r)^3$ as might be expected for an internal source of pressure.

Surface Profile

Figure 8 illustrates the profiles after each successive sintering cycle; these are examples where ρ_a/ρ_m was persistently < ρ_{oa}/ρ_{om} (case of a higher density agglomerate placed in compression by a lower density matrix). The broken lines represent the agglomerate's perimeter. This figure shows that as sintering proceeds, the agglomerate protrudes above the matrix's surface. The extent of the protrusion was proportional to both ρ_{oa}/ρ_{om} and temperature. The agglomerate also develops a crown.

The differential strain ($\Delta\varepsilon = \varepsilon_m - \varepsilon_a$) was compared to the total protrusion height (X) and the height excluding the crown (Y) as shown in Fig. 9. The shaded lines in this figure represent the protrusion height of the agglomerates that would be expected without any interaction with the matrix ($Y = R_o\ \Delta\varepsilon$, where R_o = initial agglomerate radius). As shown, the protrusion height exceeded that expected by 50% to 100%.

The extent of the extra protrusion is approximately equal to the crown height, (X-Y). It is obvious that differential strain produced by differential sintering produces a nonsymmetric stress field which results in a net force applied to the surface agglomerate. This net force pushes the agglomerate through the surface in a way which is somewhat analogous to squeezing a slippery bar of soap.

The differential strain also causes the matrix adjacent to the agglomerate to uplift. It was observed that the uplifted matrix would occasionally break away (e.g., Fig. 8, 1300°C) from the agglomerate and sinter faster than its surrounding matrix material. This phenomenon would produce a depressed surface at $r/R \approx 2$ (as shown in Fig. 8, 1400°C). After breaking away and relaxing, the matrix adjacent to the agglomerate again becomes uplifted (Fig. 8, 1450°C) due to differential sintering. As shown in the next section, this uplifting, breaking away and uplifting cycle produces two types of cracks during sintering.

SC82-16047A

SC5295.2AR

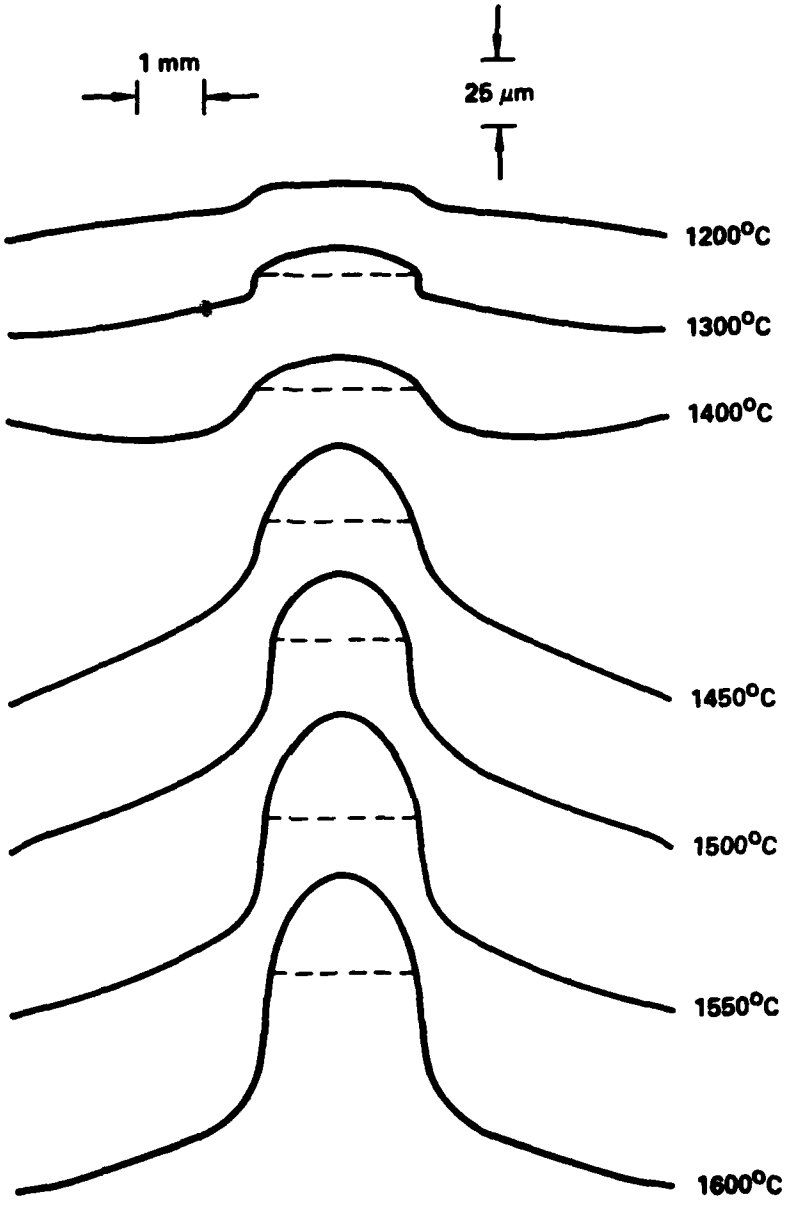

α - Al_2O_3/ZrO_2, ρ_{oa} = 0.58 ρ_t, ρ_{om} = 0.48 ρ_t

SPECIMEN 16

Fig. 8 Surface profile after each sintering cycle, an example where $\rho_a/\rho_m < \rho_{oa}/\rho_{om}$ (4).

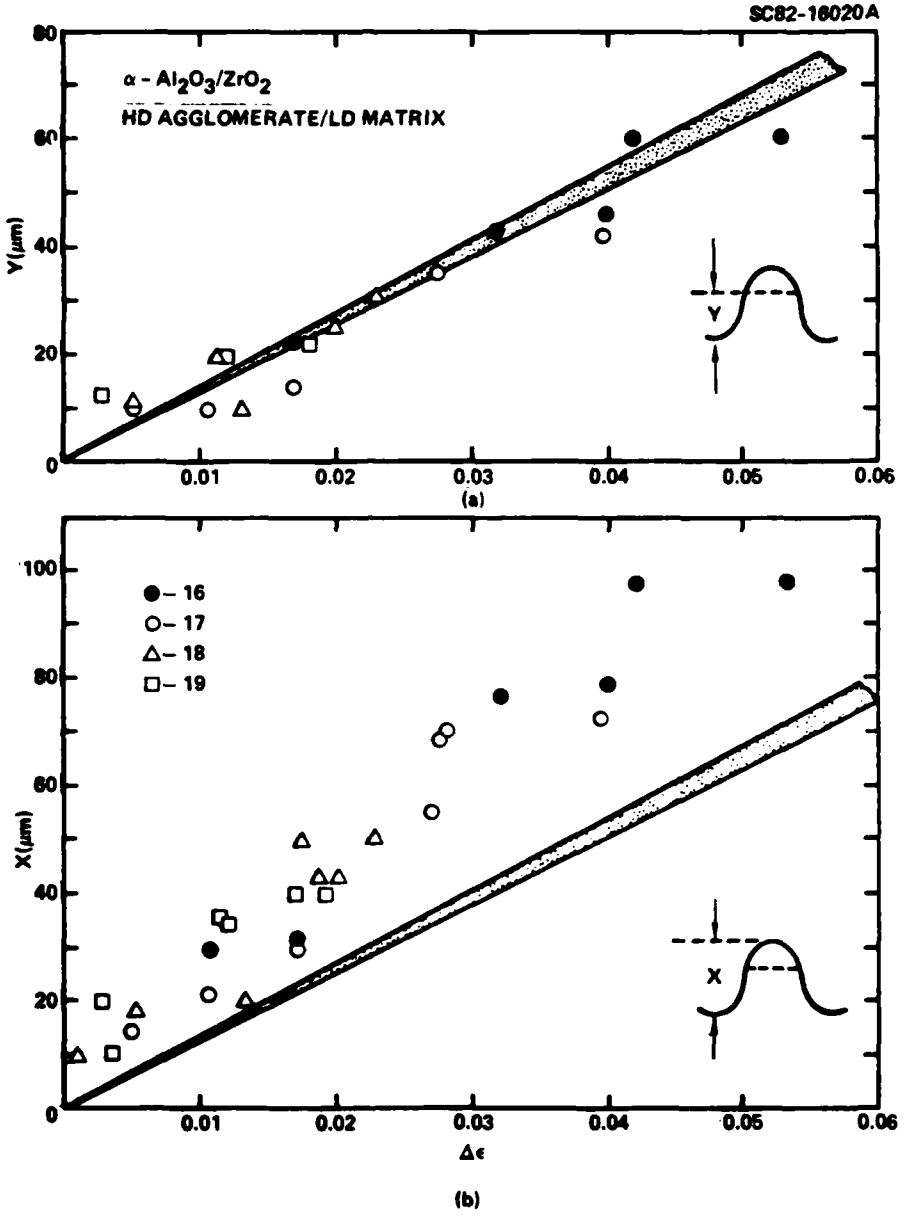

Fig. 9. Protrusion and crown heights vs differential strain (4).

For the case of the presintered agglomerates, the largest protrusion occurred during the initial heating to 1200°C, coinciding with the largest compressive strain (see Fig. 6b). As expected from the data shown in Fig. 6b, the protrusion height decreased with increasing temperature. For the specimens

where ρ_a/ρ_m became > ρ_{oa}/ρ_{om} near the end of the cyclic sintering schedule, the agglomerates became depressed below the matrix surface.

Cracks Produced by Differential Sintering

Figure 10 illustrates the typical circumferential crack developed at the agglomerate/matrix interface for the case of a lower density (and faster sintering) surface agglomerate within a higher density matrix. (These specimens were fabricated by a route that did not require agglomerate presintering.)

Figure 11 illustrates the circumferential type of crack developed for the case where the agglomerates were presintered and the end-point ρ_a/ρ_m was > ρ_{oa}/ρ_{om} (i.e., the agglomerates were under compression during most of the sintering schedule, but shrank away from the matrix near the end of the sintering schedule).

SC82-15945A

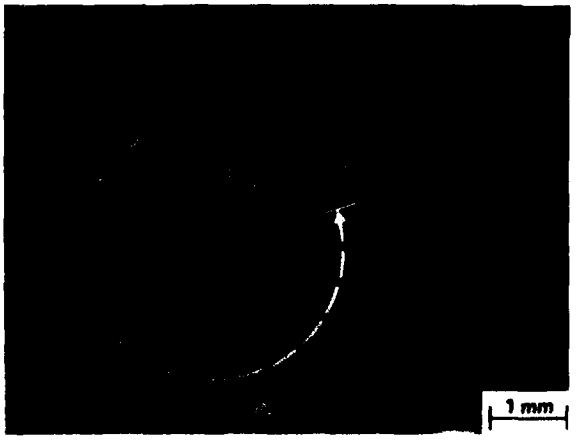

Fig. 10. Circumferential crack developed at agglomerate/matrix interface; case where $\rho_{oa}/\rho_{om} < 1$ and agglomerate were not presintered (4).

SC82-16813

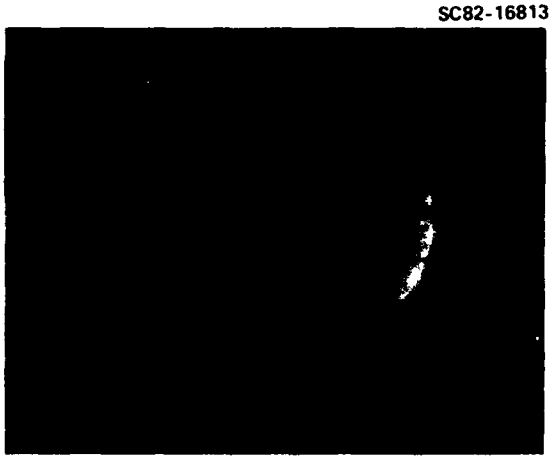

Fig. 11. Circumferential crack developed when matrix breaks away after agglomerate protrusion (4).

Four types of crack-like separations were observed in specimens containing the higher density surface agglomerates. The first type was similar to that shown in Fig. 11, but occurred when the matrix adjacent to the uplifted

agglomerate broke away. The second type is shown in Fig. 12. This lateral crack, which circumvented the bottom of the agglomerate, forms after the adjacent matrix breaks away and relaxes, and then becomes uplifted for the second time. Figure 12 also shows the partially healed crack at the agglomerate/matrix interface produced by the breakaway condition discussed above.

The third type of crack is shown in Fig. 13. Here radial cracks are produced by the tangential tensile stresses developed in the matrix adjacent to the agglomerate. These cracks were only observed when $1.02 < \rho_{oa}/\rho_{om} < 1.05$, i.e., when the differential density was small, but the matrix still exerted a compressive stress on the agglomerate, without producing an extensive protrusion.

SC82-15943

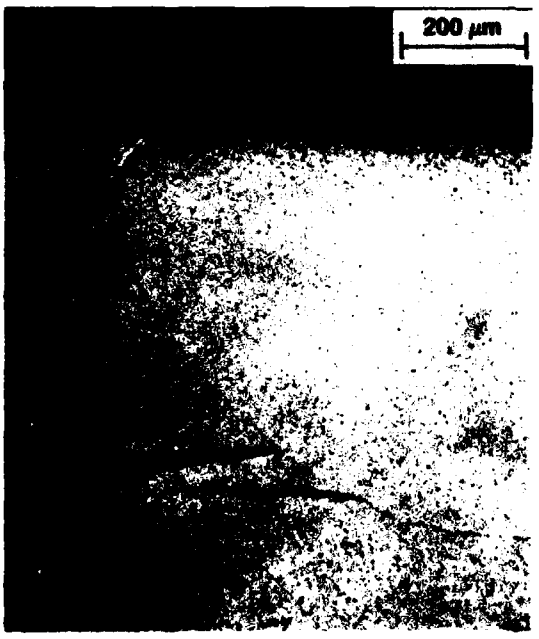

Fig. 12 Lateral crack which circumvents bottom of agglomerate (4).

SC82-15947A

Fig. 13 Radial cracks due to tangential stress in matrix (4).

The fourth type of crack was observed to transverse the top portion of the agglomerate; i.e., to cut through the crown formed on the agglomerate. This type of crack apparently formed to relieve tensile stresses in the crown.

Colloidal Routes to Strengthening[6]

The review above has shown that agglomerates in a consolidated powder produce crack-like voids. Since agglomerates are inherent to dry-powder consolidation routes, it is obvious that other consolidation routes with the potential of avoiding agglomeration must be sought. Colloidal systems have this potential. In colloidal systems, sponatenous agglomeration can be avoided by producing repulsive forces beween particles either electrostatically or sterically. Well dispersed particles within a colloid can be consolidated by filtration, gravitation or centrifugal settling, evaporation and electrophoresis. It was reasoned that if agglomerations could be avoided up to the last moment of particle consolidation from the colloid, the uniformity of the consolidated state would reflect the uniformity of the colloidal state.

The composite composition chosen for this study included 30 volume % (v/o) ZrO_2 with 2.2 mole % (m/o) Y_2O_3 since previous work has demonstrated that at this composition tetragonal ZrO_2 could be fully retained to achieve significant toughening and strengthening.

Commercial grade powders of Al_2O_3 (A-16SG#), and ZrO_2 (2.5 m/o Y_2O_3) were used. Ball-milling was necessary to break up the hard agglomerates. Milling in water at pH = 2.0 was done with high-alumina balls in a high-alumina jar. The effect of milling on dispersion was monitored through particle/agglomerate size distribution measurements.

pH adjustments, with the addition of reagent grade HCl, were made until ball-milled suspensions of either Al_2O_3 or ZrO_2 (2.2 m/o Y_2O_3) displayed maximum dispersion by particle size distribution measurements. In both cases, the maximum dispersion was achieved at pH = 2.0 - 2.5. The composite Al_2O_3-ZrO_2 suspensions were then similary dispersed in this pH range. For this condition the average particle/agglomerate size was 0.6 μm. Composite suspensions were prepared with solid contents less than 35 v/o.

Gypsum mold (prepared by mixing gypsum powder with water at a weight ratio of 100:75) were used as the filtering medium. The green density of the A-16SG + ZrO_2 composite powder varied between 50 - 55% of the theoretical density. Filtered discs of the composite were dried and sintered at 1600°C/ 2 hrs in air

to obtain a density of 98% of theoretical. The residual porosity was associated with relatively small (< 10 μm) ZrO_2 hard agglomeratesd similar to that shown in Fig. 4.

Flexural strength measurements were obtained by four-point bending (inner span = 1.27 cm, outer = 2.54 cm) with diamond cut and ground (220 grit) specimens. The average strength was 896 MPa vs 550 MPa for the same powders processed with a dry consolidation route. An amorphous third phase was observed at the fracture origin suggestive of impurities picked up during milling.

SUMMARY REMARKS

Within the scope of the work reviewed, it has been shown that sintered materials can fail from crack-like internal surfaces. The results concerning the differential sintering of agglomerates relative to their matrices show that a variety of crack-like voids are produced where the green density of the agglomerate is different (either higher or lower) than its surrounding matrix. Since strength is inversely proportional to the square root of the crack size, and the crack size is proportional to the agglomerate size, one must conclude that the strength of a sintered ceramic is, in part, inversely proportional to the square root of the size of the agglomerates in the consolidated powder. That is, the strength potential of a sintered ceramic is directly related to processing variables which control agglomerate size (i.e., powder manufacture, powder processing and consolidation method).

From a sinterability standpoint, it should be noted that the crack-like voids produced by differential sintering limit end-point density. The fraction of porosity (P) produced by differential sintering can be related to the volume fraction (V_a) of low density agglomerates with

$$P = \left[\frac{\rho_{om} - \rho_{oa}}{\rho_t}\right] V_a \quad .$$

With this simple relation, conditions can easily be perceived where $0.01 > P > 0.10$.

It has also been shown that the matrix can exert compressional stresses on the agglomerate when it densifies faster than does the agglomerate. When this stress field is nonsymmetric, as it is for the surface agglomerate, it promotes agglomerate mobility (i.e., tends to push the agglomerate out of the surface). If a completely submerged, high density agglomerate were surrounded by a matrix with a nonuniform green density, the resulting stress field would also be nonsymmetric and its net force would also cause agglomerate motion.

Mass rearrangement by agglomerate motion takes place over much greater distances within the same time frame than can ever be expected through diffusional processes. More open, lower green density matrices would be expected to offer less resistance to agglomerate mobility. If mass rearrangement produced by agglomerate mobility would lead to a more sinterable microstructure, it would explain why lower green density compacts initially exhibit greater densification rates.

The observations reviewed here reinforce current thinking that agglomerates must be eliminated from powders. Colloidal routes to processing are effective in removing soft agglomerates as demonstrated by strengthening results by colloidal/filtration.

ACKNOWLEDGEMENT

This work was supported by an Air Force Office of Scientific Research Contract No. F49620-81-C-0036.

REFERENCES

1. T. A. Wheat, J. Can. Ceram. Soc. 40 (1971) 43.
2. H. E. Exner Rev. Pow: Met and Phys. Chem. 1[1-4] (1979) 124.
3. F. F. Lange "Processing Related Fracture Origins: Part 1, Observations in sintered and HIP Treated Al_2O_3/ZrO_3 Composites," J. Am. Ceram. Soc. (in Press).
4. F. F. Lange and M. Metcalf, "Ibid: Part 2 Agglomerate Mobility and Crack-Like Internal Surfaces Caused by Differential Sintering," J. Am. Ceram. Soc. (in Press).
5. C. A. Bruch, Bul. Am. Ceram. Soc. 41 (1962) 799.
6. I.A. Aksay, B.I. Davis and F.F. Lange, "Development of Uniformity in Al_2O_3-ZrO_2 Composites by the Colloidal/Filtration Route to Consolidation," J. Am. Ceram. Soc. (in Press).

APPENDIX II

STRESSES INDUCED BY DIFFERENTIAL SINTERING IN POWDER COMPACTS

Rockwell International
Science Center

SC5295.2AR

STRESSES INDUCED BY DIFFERENTIAL SINTERING IN POWDER COMPACTS

Bruce Kellett

Department of Material Science and Engr.
School of Engr. and Applied Science
University of California
Los Angeles, CA 90024

and

F. Lange

Rockwell International Science Center
Thousand Oaks, CA 91360

ABSTRACT

Stresses created by differential sintering, due to differences in initial bulk density, were determined experimentally. The experiments entailed determining the shrinkage rates of a powder isostatically pressed to two different bulk densities. Using this information, stresses were determined by forcing the slower densifying compact to shrink at the same rate as the faster densifying compact and measuring the resulting forces with a load cell. Maximum stresses (between 200 and 400 psi) were observed to occur in the intermediate stage of densification. Despite larger differential strains at higher temperatures, stresses decreased to zero at the latter stage of densification. Viscoelastic experiments, of the stress relaxation type were performed. Results showed that the sintering specimen was more rigid at lower temperatures and more fluid-like at higher temperatures, to explain the development of maximum stresses at intermediate temperatures.

INTRODUCTION

The processing of ceramics is currently the focus of much attention. Based on recent work in the area of fracture mechanics, researchers now feel that great improvements in the fracture strength of ceramics are possible with improved processing. These improvements hinge upon the ability of the ceramist to eliminate flaw populations inherent to certain processing methods. Agglomerates produced a major flaw population by causing crack-like voids to form by differential sintering.[1,2] Agglomerates produce inhomogeneous density distributions which can carry through to the sintered body as crack-like voids.

Sintering kinetics are dependent on bulk density, therefore any agglomerated powder compact will show shrinkage variations from one small region to the next as shown by Fig. 1. Lower green density compacts densifies faster than a higher green density compacts[3,4] and occupy less volume after complete densification. The corresponding differential strains are expected to give rise to stresses within the sintering powder compact during sintering.

Any calculation used to determine these stresses would have to consider microscopic details of agglomerates, their local shrinkage behavior and their stress-strain behavior over the period of densification. We attacked this problem on a more tractable macroscopic level. The powder compact was considered as composed of a higher density agglomerate surrounded by a powder matrix of lower density. To determine this maximum stress, the shrinkage rate of powder compacts of two different bulk densities were measured at constant heating rate. The slower densifying compact was then forced to densify at the same rate as the faster densifying compact within a mechanical test machine that measured the resulting force. In this manner, the stress arising from differential sintering was determined over the full range of heating with only one assumption concerning the stress-strain behavior of the densifying powder compact, viz both the low and high bulk density compacts exhibit very similar viscoelastic behavior.

SC82-19336

Fig. 1 Density variations produced by iso-pressing dry powder (sintered to ~90% of theoretical density).

Procedures

A composite powder consisting of 70% Al_2O_3* and 30% ZrO_2** was used for this study. An equivalent of 2 mole % Y_3O_3 was added to the ZrO_2 as $Y(NO_3)_3$.*** The material was ball milled in methanol with high alumina balls in a polyethylene container overnight, flash evaporated, and then calcined at 600°C overnight to convert the $Y(NO_3)_3$ to Y_2O_3. The composite power was ground with a mortar and pestle, and then axially pressed (4000 psi) into cylindrical specimen (1 in. by 1/3 in. dia.). The cylindrical compacts were isostatically pressed at 10 and 50 ksi to produce specimens with densities of 2.22 and 2.63 g/cc, respectively.

Compacts were sintered in air. Shrinkage measurements for both the high and low bulk density compacts were obtained for heating rates of 5, 10, 20°C/min (between 900°C and 1550°C) using an extensiometer described elsewhere.[5] Results, expressed as dimensionless strain ($\varepsilon = \Delta\ell/\ell_0$), were obtained with three or more specimens for each bulk density and for each heating rate.

To determine the sintering stresses, a high green density specimen which exhibited the slower shrinkage rate, was placed in a furnace between SiC rods attached to the moving crosshead of a mechanical testing machine.§ During heating the crosshead was moved to mimic the displacement rate of the lower green density compact. The thermal expansions of the load train had to be experimentally determined and subtracted from the applied displacement rate. These expansions were experimentally determined for the two heating rates (5 and 10°C/min) used to determine stresses. This was accomplished by determining the displacement rate required to maintain a constant applied load on the load train during heating at the desired heating rate.

Each constant heating rate experiment was initiated at 900°C. A displacement rate was applied to the specimen which forced it to shrink at the rate

*ALCOA A16 superground
**Zircar, Inc.
***Research Chemical, Inc.
§Instron

as the lower green density compact. This displacement rate was determined for each heating rate by subtracting the expansion history of the loading train from the shrinkage history determined by experiments describe above. An extensiometer (see Fig. 2) was used to ensure that the correct displacements were applied.

Viscoelastic experiments of the stress relaxation type were performed to determine the changing nature of the sintering body as a function of temperature. These experiments required the same apparatus as described above for the sintering stress experiments. The tests were performed at temperatures between 1000°C to 1550°C using a high green density specimen which was sequentially tested from low to high temperature. The relaxation experiments entailed quickly applying a very small compressional strain to the specimen to obtain an initial stress between 200 psi to 1000 psi, depending on temperature. The initial stress was allowed to dissipate at constant strain. Since these tests caused only a slight compressional strain, negligible densification occurred. The powder compact was modeled as a Maxwell element with the spring acting as the compact's elastic skeleton and the dash pot corresponds to its viscous processes (sintering and deformation). The characteristic relaxation time λ was determined from the time taken for the stress to decay to 1/e of its initial value. The characteristic relaxation time is a measure of the compact's viscosity to elastic modulus ratio.

RESULTS

As shown by the example in Fig. 3 (heating rate = 5°C/min), the lower green density compact always showed greater shrinkage strains relative to the higher green density compact. Shrinkage at all heating rates initiated ~ 1000°C. Differential shrinkage between the high and low density compacts was sufficiently significant to be observed began at about 1050°C.

Shrinkage rates were determined graphically as a function of temperature. As shown in Fig. 4, the shrinkage rate peaked at high temperature

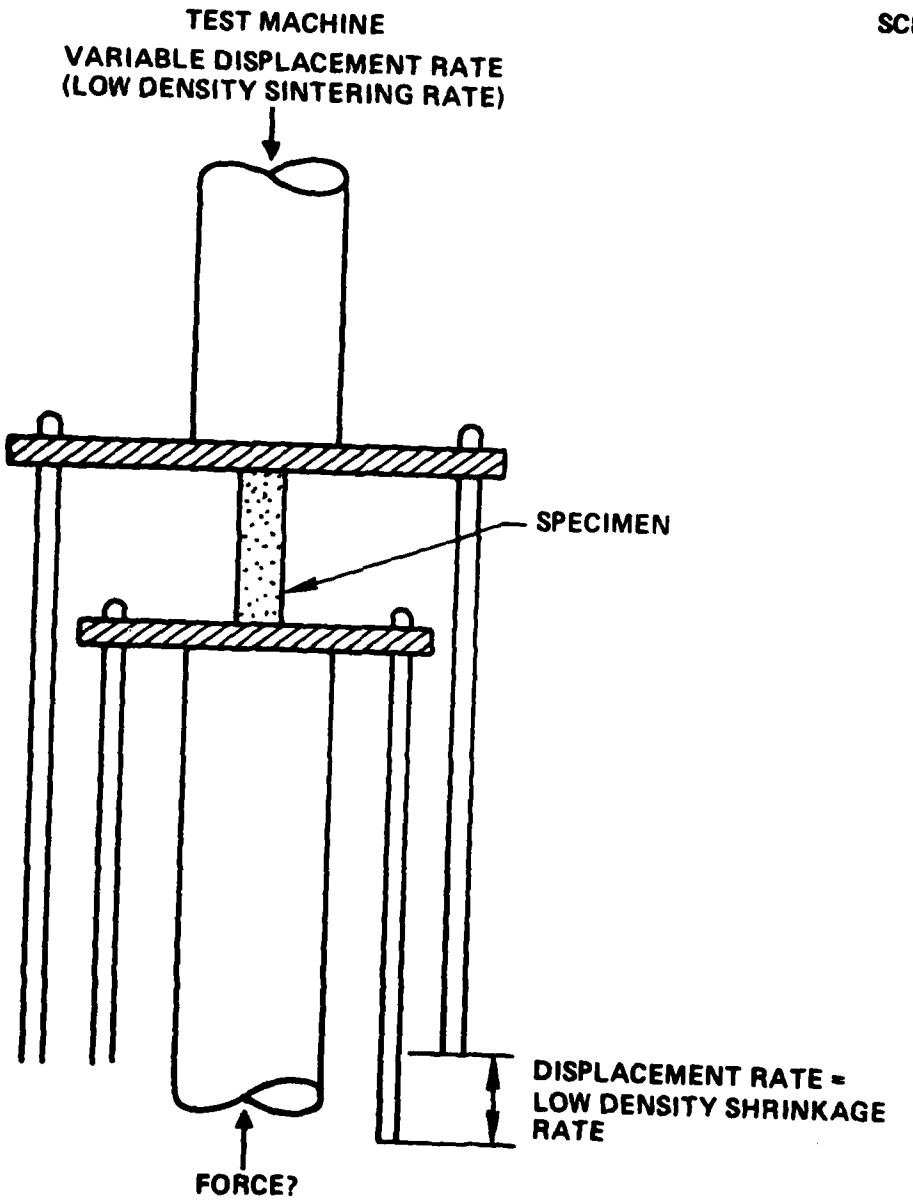

Fig. 2 Schematic of the loading train and extensometer used to force the higher green density specimen to sinter at the same rate as the lower green density material.

SC82-19338

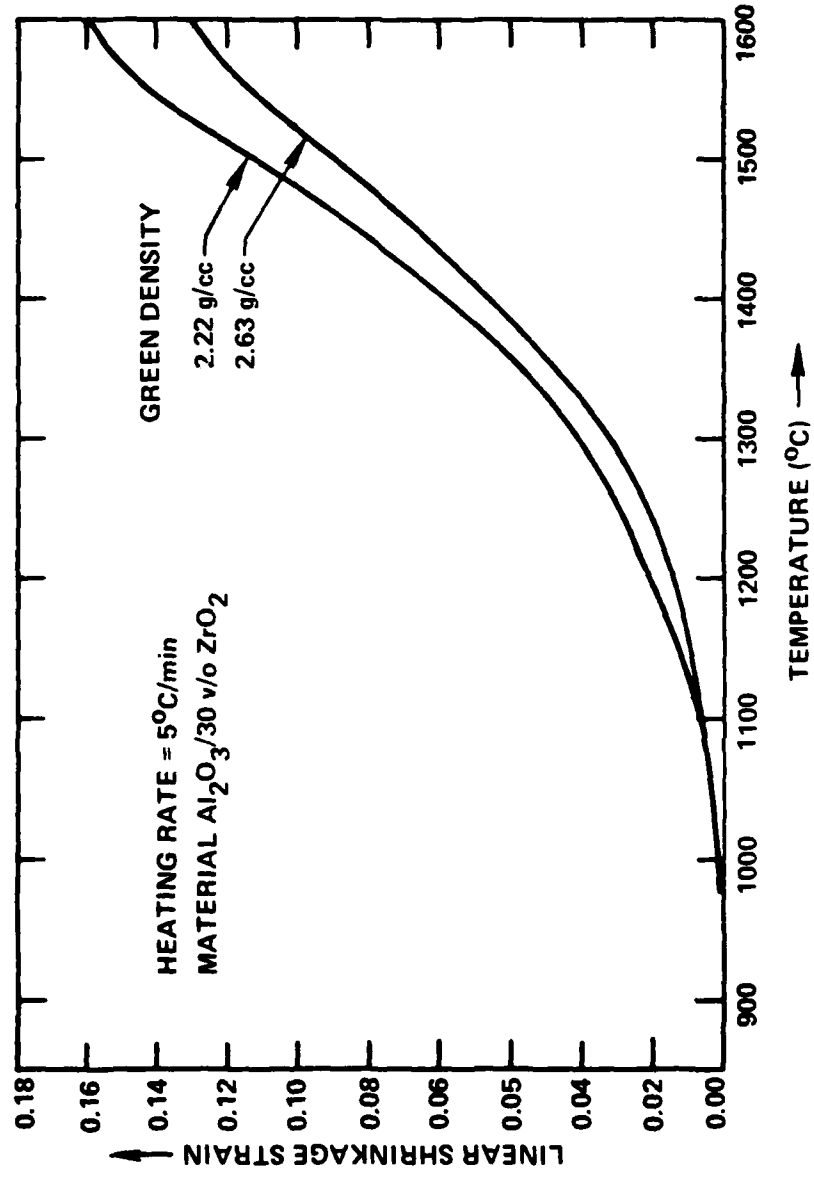

Fig. 3 Shrinkage strain vs temperature for two composite powders with different initial bulk densities (2.22 gm/cc and 2.63 gm/cc) heated at 5°C/min.

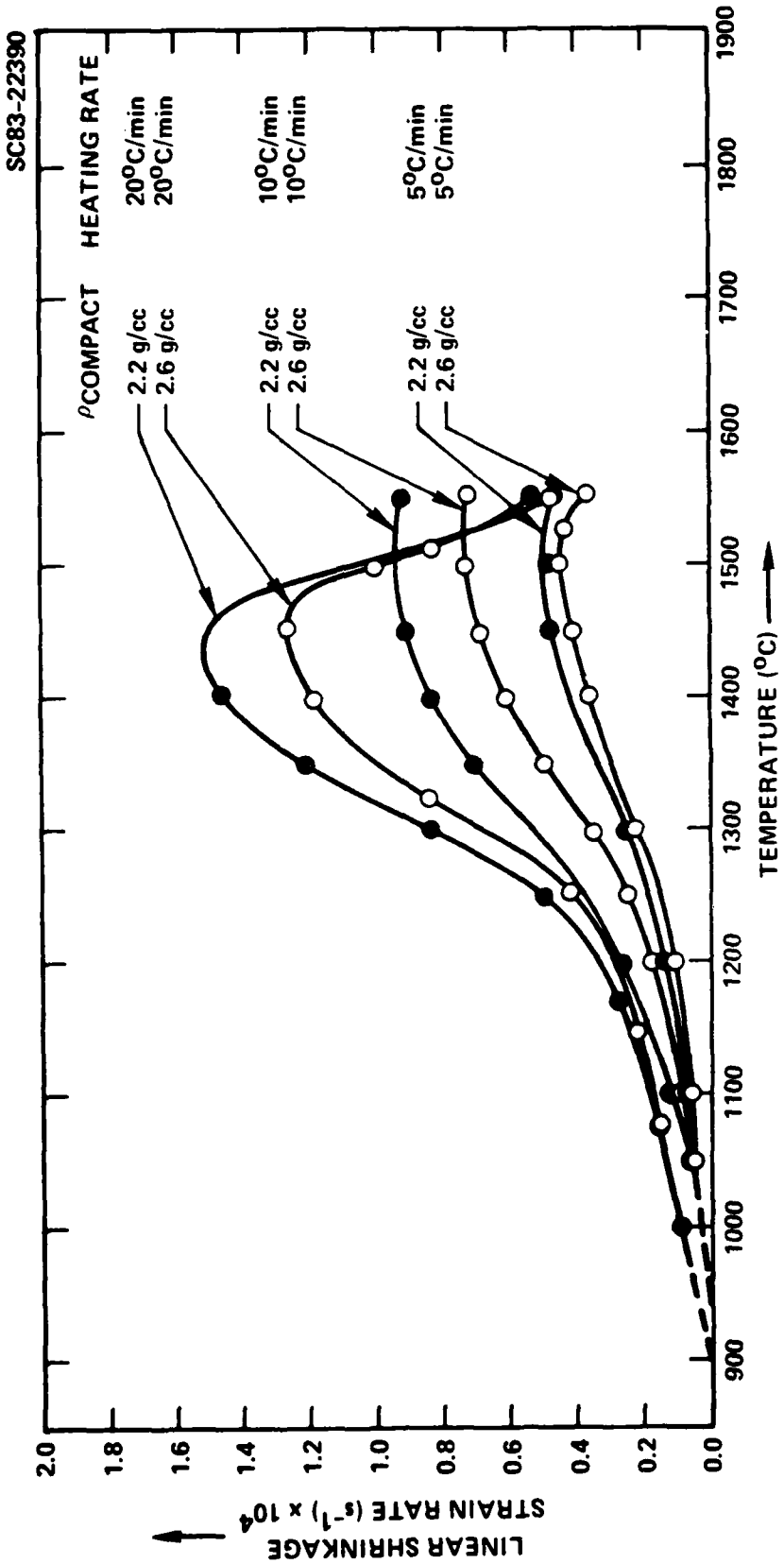

Fig. 4 Shrinkage strain rate vs temperature for high and low green density compacts heated at the three heating rates.

(> 1450°C), was greater for faster heating rates, and was greater for the low density compact relative to the higher density compact for a given heating rate. The differential shrinkage rate between the two different density compacts was the greatest at 1550, 1500 and 1435°C for heating rates of 5, 10 and 20°C/min, respectfully. Conversion of the linear shrinkage data into density ($\rho = \rho_0/(1 - \varepsilon)^3$, where ρ_0 is the initial green density) showed that the higher green density compact was always denser than the low density compact despite its lower shrinkage rate as shown in Fig. 5.

Experiments to determine the stress produced by differential shrinkage were performed at heating rates of 5 and 10°C/min. Figure 6 illustrates these data. Although the form of the data were consistent from one specimen to the next, individual experiments produced different stresses. The data scatter between experiments was caused by slight, but consistent deviations in the applied crosshead displacement rates relative to the displacement rates which exactly mimic the shrinkage rate of the low density compact. For this reason, the maximum stress could only be estimated as ranging between 200 and 400 psi and no differences could be observed for the two heating rates. As shown in Fig. 6, the stresses increase to a maximum value at ~ 1200°C and then dissipate to ~ zero at 1500°C.

Results of stress relaxation experiments are shown in Fig. 7. As illustrated, the characteristic relaxation time decreased by ~ 3 orders of magnitude between 1000°C and 1500°C. At temperature > 1400°C, data was difficult to obtain since stresses relaxed nearly as fast as they were applied. Thus, in general, the viscoelastic compact can be described as an elastic body at low temperatures and a viscous body at high temperatures.

DISCUSSION

As observed here and by others,[3,4] lower green density compacts exhibit a greater shrinkage and shrinkage rate over the full range of sintering. As demonstrated here, the differential shrinking produced by a green density differential of ~ 0.4 gm/cc (2.22 gm/cc vs 2.63 gm/cc) results in maximum

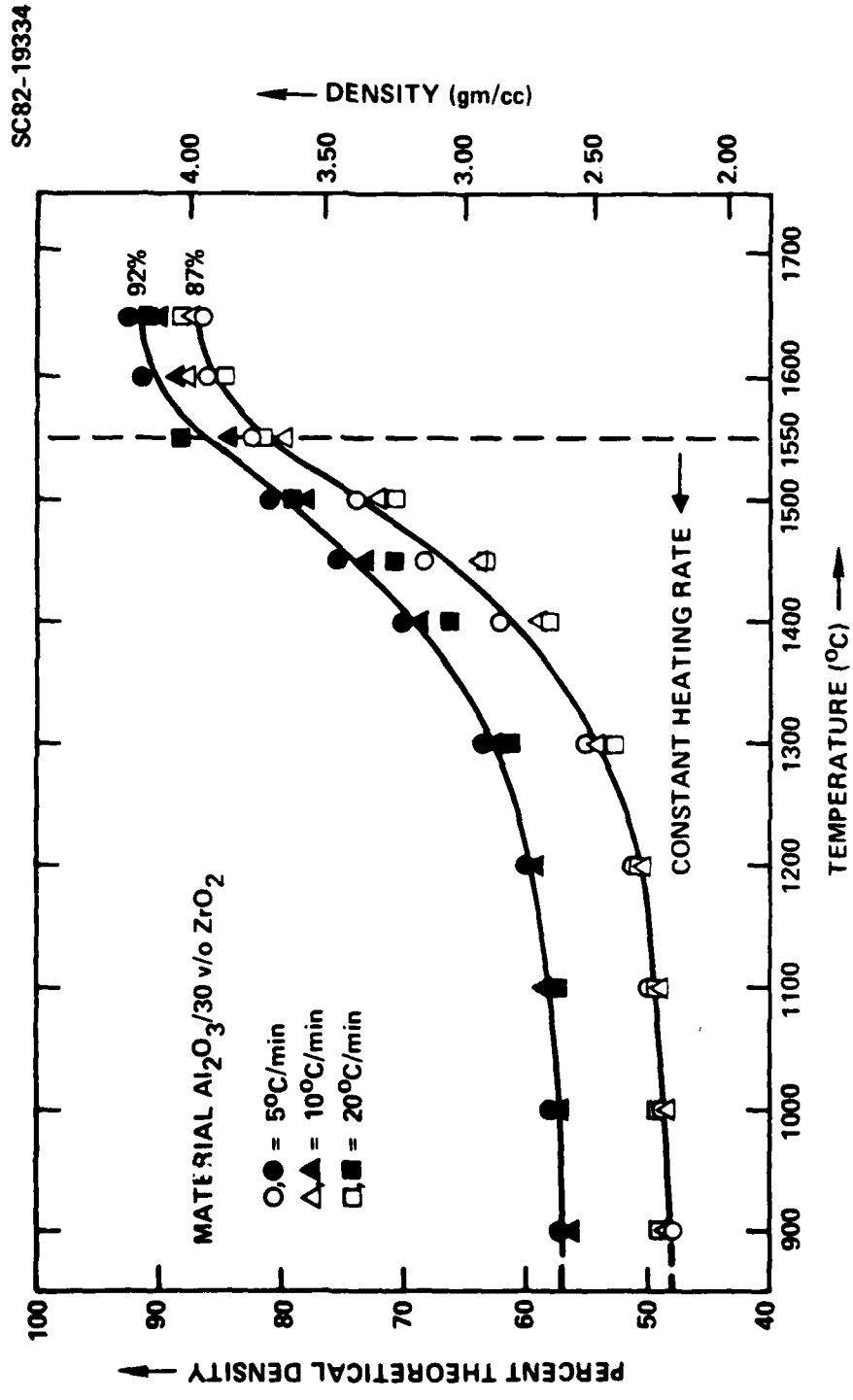

Fig. 5 Relative density vs temperature for both high and low green density compacts sintered at the three heating rates.

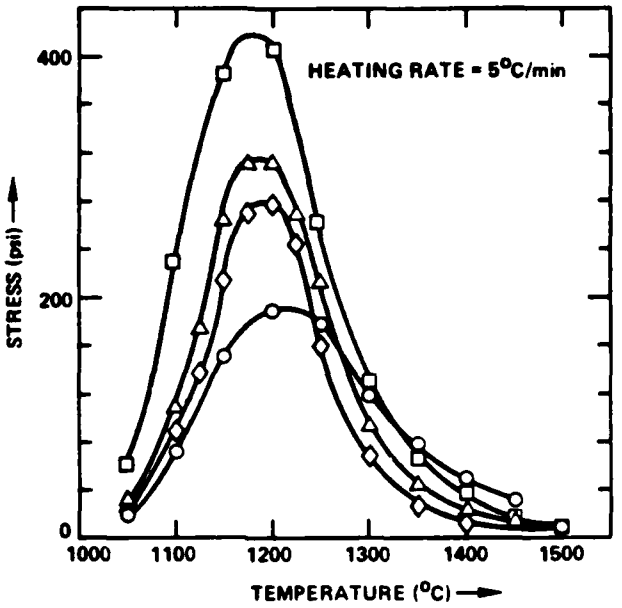

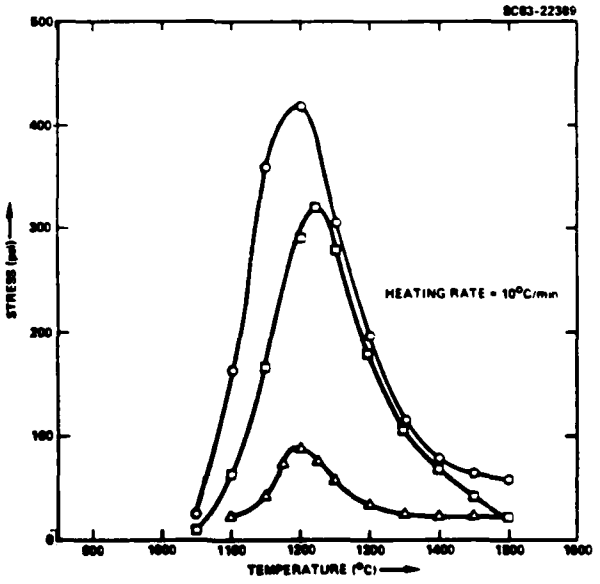

Fig. 6 Stresses resulting from forcing the high green density compact to shrink at the same rate as the lower green density compact: a) heating rate of 5°C/min and b) 10°C/min.

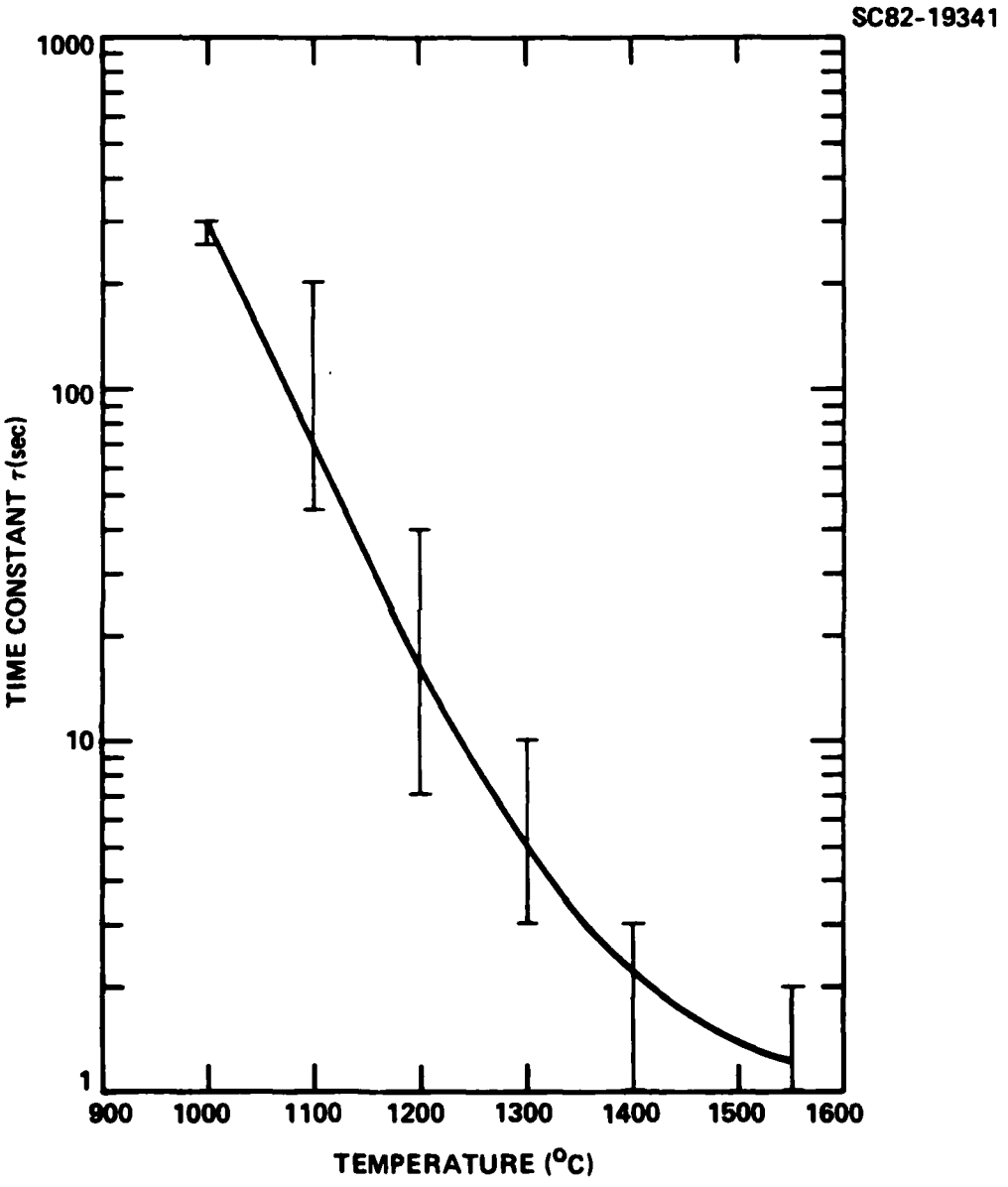

Fig. 7 Characteristic relaxation time constant vs temperature.

stresses ranging between 200 and 400 psi for the heating rates studied. Although the maximum differential strain and differential strain rates occurred at high temperatures (> 1450°C), the maximum stress occurred at relatively low temperatures (~ 1200°C). Stress relaxation experiments strongly suggest that the maximum stress arises at lower temperatures because the material is more elastic, whereas at high temperatures, stresses can quickly dissipate.

Since the densifying powder compact exhibits viscoelastic behavior over its complete range of densification (see Fig. 7), one would expect that the magnitude of the stresses would be proportional to the strain rate, which as shown in Fig. 4, is proportional to the heating rate. That is, the maximum stress developed due to differential sintering might be minimized by heating at a slower rate over the critical temperature range (~ 1200°C for case examined here). Unfortunately, the accuracy of the current experiments did not permit any correlation between heating rate and maximum stress.

One might ask: is 200-400 psi sufficient to produce the crack-like voids observed by the differential sintering of agglomerate/matrix systems?[4] The answer is beyond the scope of the present work, but it might be pointed out that in model studies, the crack-like voids were observed to occur during the initial stage of sintering where the powder compact is expected to be weakest.

ACKNOWLEDGEMENTS

This work was supported by the Air Force Office of Scientific Research, Contract F49620-81-C-0036.

REFERENCES

1. K.D. Reeve, "Non-Uniform Shrinkage in Sintering," Bul. Am. Ceram. Soc. 42, [8] 452 (1963).

2. F.F. Lange, "Processing Related Fracture Origins: Part 1, Observations in Sintered and HIP Treated Al_2O_3/ZrO_2 Compositions," J. Am. Ceram. Soc. (in press).

3. C.A. Bruch, "Sintering for the High Density Alumina Process," Bul. Am. Ceram. Soc. 41 799 (1962).

4. F.F. Lange and M. Metcalf, Ibid Ref. 2 "Part 2: Agglomerate Motion and Crack-Like Internal Surface Formation due to Differential Sintering"

5. F.F. Lnage, B.I. Davis and D.R. Clarke, "Compressive Creep of Si_3N_4/MgO Alloys: Part 1 Effect of Composition," J. Mat. Sci. 15 601 (1980).

APPENDIX III

SOME PROCESSING REQUIREMENTS FOR TRANSFORMATION TOUGHENED CERAMICS

SOME PROCESSING REQUIREMENTS FOR TRANSFORMATION TOUGHENED CERAMICS

F. F. Lange

Rockwell International Science Center
Thousand Oaks, CA 91360

and

Nils Claussen

Max-Planck Institut fur Metallforschung
7000 Stuttgart 80, F.R.G.

1. Introduction

Investigators, like ourselves, who have been interested in validating concepts concerning mechanical reliability, have had, by necessity, to fabricate our own materials to achieve certain microstructures of interest. As described below, many of the interesting concepts involve two-phase microstructures and the need to control the size and distribution of the individual microstructural features. In attempting to fabricate these microstructures, one quickly learns that powders, powder processing and densification processes are controlling, and in many cases, limiting parameters.

Concepts that have been shown to improve strength will be emphasized. These concepts may be directly related to processing, e.g., crystal structure of powder, agglomerates within powders, or indirectly related to processing via certain restrictions, e.g., restrictions on the particle size, grain size, etc. required to achieve small crack size, high toughness, etc. Strength (σ_s) is determined by fracture toughness (as measured by the critical stress intensity factor, K_c) and the size of the crack that initiates failure (c):

$$\sigma_s \propto \frac{K_c}{\sqrt{c}} \quad .$$

Thus, this review will divide the concepts into two parts - those processing parameters related to decreasing crack size, and those related to retaining

tetragonal ZrO_2, the toughening agent, in materials that exhibit a phenomena known as transformation toughening.

2. Control of Crack Size

Fracture origins in virgin ceramics are in some way related to inhomogeneities introduced during fabrication (powder manufacture, processing, sintering, and subsequent machining). The average size,* size distribution and type of inhomogeneity determines average strength, strength distribution and changes in fabrication procedures required to increase structural reliability. The poor reliability of current ceramics is primarily due to their large and unpredictable strength distributions that stems from the unpredictable distribution of inhomogeneities introduced during fabrication. Identification of the fabrication step that produces the strength degrading inhomogeneity and the fabrication and/or microstructural changes required to eliminate the inhomogeneities (or reduce their size) is critical to improving the structural reliability of ceramics.

There are a large number of different types of inhomogeneities, which space and knowledge would not warrant categorizing here. Some are specific to a given processing route, e.g., air pockets produced during injection molding and slip casting. Others depend on powder handling and processing environments, e.g., voids left by lint. The three described below, viz. crack-like voids produce by agglomerates, inclusions and large grains are not only common to all powder routes, but also give insight to some characteristics required of a powder, and why two-phase systems can be highly desirable.

Crack-Like Voids Produced by Agglomerates

Agglomerates are common to all powder processing routes. They can be classified as either soft, i.e., particles held together by van der Waals forces which can be broken apart with surfactants, or hard, i.e., partially sintered groups of particles which require attrition to dismember. All dry powders

*Adjusted to the propensity of the inhomogeneity to degrade strength.

contain soft agglomerates. Hard agglomerates are common to powder manufacturing routes that involve calcining. Some processing routes (spray drying) purposely form large agglomerates to produce a flowable 'powder' for dry pressing.

Figure 1 illustrates the macrostructure of a dry iso-pressed powder sintered to 90% of theoretical density. As shown, the soft agglomerates are retained during consolidation to result in an inhomogeneous density distribution within both the green and nearly dense states. It has been shown that fully dense bodies fail from crack-like voids produced by the differential shrinkage of the agglomerate relative to its surrounding consolidated powder matrix. Figure 2 schematically shows two extreme cases which have been confirmed by direct observations on model systems.[1] Figure 2a is the case where the low green density agglomerate shrinks away from its surrounding higher density matrix to form a circumferential, crack-like void. Figure 2b is the case where the low green density matrix shrinks upon a higher density agglomerate to produce radial, crack-like voids. In both cases, the size of the crack-like void is proportional to the agglomerate size.

The crack-like voids can be eliminated (or reduced in size) by two methods. First, the crack-like voids present in the near theoretically dense (> 98%) bodies can be closed by hot-gas isostatic pressing (HIPing). HIP treatment can significantly increase the strength of a Al_2O_3/ZrO_2 sintered body (500 MPa for sintered to 875 MPa for sintered and HIP'ed).[1]

The second approach is more fundamental to processing science. It involves dispersing the powder(s) in a liquid containing a surfactant which eliminates the soft agglomerates and consolidating the powder from the colloidal state to form the desired engineering shape which is dried and sintered.[2] The colloidal route can also be used to obtain uniform dispersions of two or more phases. As shown in Fig. 3 (case of a Al_2O_3/ZrO_2 composite), hard agglomerates cannot be broken apart with surfactants; these hard agglomerates produce crack-like, circumferential voids due to differential shrinkage. The colloidal route can still be used to eliminate hard agglomerates greater than a given size by sedimentation.[1] Using the colloidal route, both single phase transformation toughened (TT), tetragonal ZrO_2 (+2.2 m/o Y_2O_3), and two phase TT Al_2O_3 v/o

SC82-19336

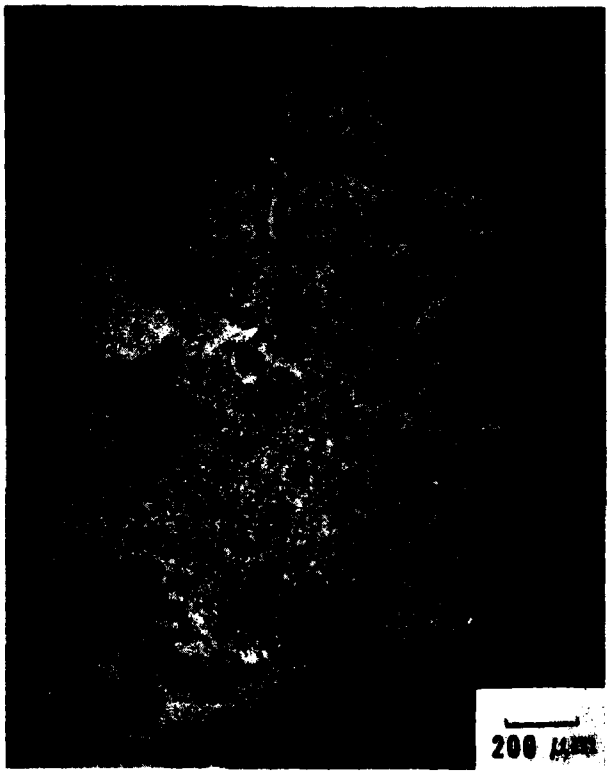

Fig. 1 Inhomogeneous density distribution for a Al_2O_3/ZrO_2 composite powder compact produced by dry iso-pressing and sintered to 90% of theoretical density.

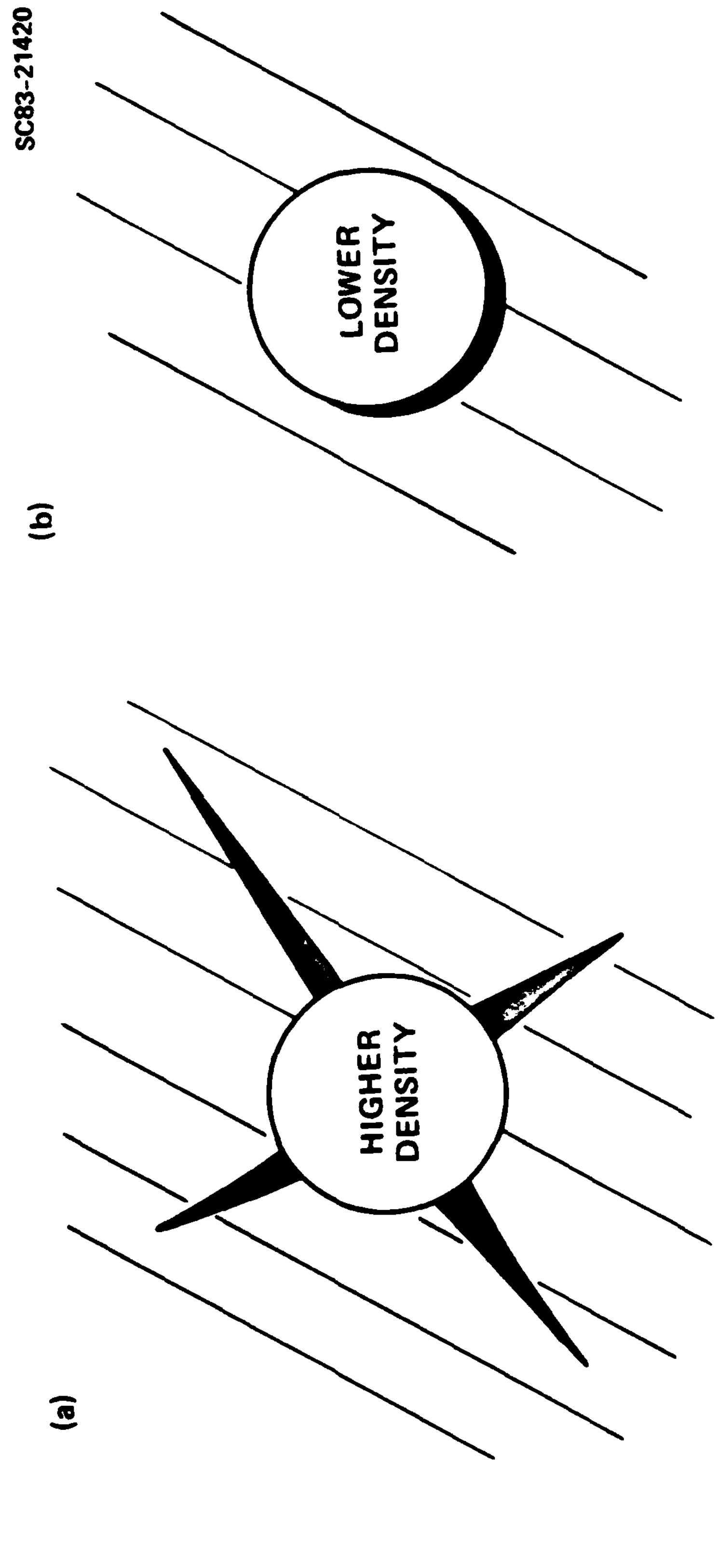

Fig. 2 Differential shrinkage during sintering due to differential green density produces a) circumferential and b) radial cracks.

SC82-16789

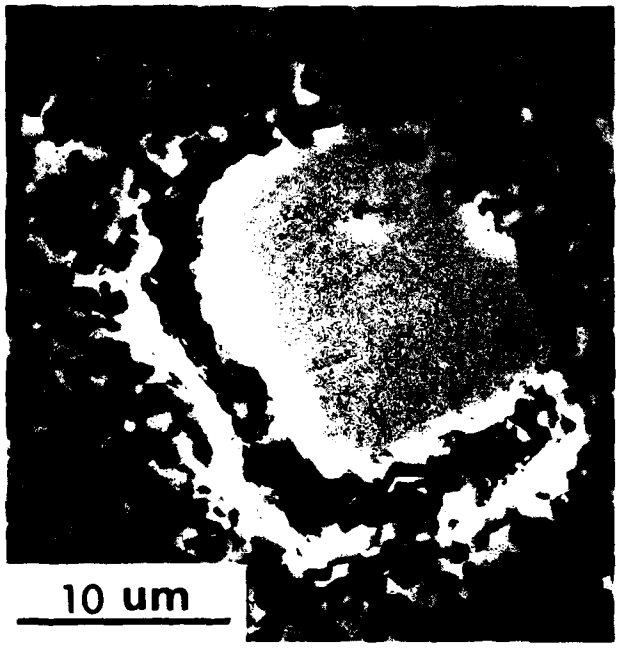

Fig. 3 Circumferential crack-like void produced during sintering by a ZrO_2 hard agglomerate in a Al_2O_3/ZrO_2 composite.

ZrO_2 (+2.2 m/o Y_2O_3) have been sintered to > 0.98 p_t to result in a mean strength > 1000 MPa (150,000 psi). Fracture origins in these stronger materials are no longer crack-like voids due to agglomerates, but voids produced by organic contaminants, such as lint.

Inclusions (Rev. Ref. 3)

Large, second phase inclusions are commonly observed at fracture origins. Such inclusion are usually contaminates introduced during powder manufacture and processing. Since the thermal expansion and/or elastic properties of the inclusion are different than the matrix phase, localized stresses develop within and around the inclusion during cooling from the fabrication temperature and/or during subsequent stressing. The distribution of these stresses are well known for simple inclusion shapes, viz. spheres and ellipsoids. The largest tensile stress arises at the inclusion/matrix interface. For the case of differential thermal contraction, the magnitude of the largest tensile stress depends on the elastic properties of the two phases, the change in temperature, and which of the two phases contacts more during cooling.

When certain conditions are met, a small preexisting flaw at the inclusion/matrix interface can extend into a large microcrack either during cooling or subsequent stressing. Similar to the agglomerate problem discussed above, the type of microcrack developed depends on whether the inclusion contracts more than the matrix (circumferential, Fig. 2a) or less than the matrix (radial, Fig. 2b). Although analyses of this problem have produced many subtle and interesting conclusions, the major conclusion is that the conditions for microcrack formation not only depends on the magnitude of the maximum tensile stress and the size of the preexisting flaw, but also on the size of the inclusion. That is, for a given maximum residual tensile stress (σ_r) microcracks will not form during cooling if the inclusion is less than a critical size, R_c^o.

Analyses concerning the effect of an added, applied tensile stress are more recent. Again, the principal conclusion is that the inclusion size also governs the formation of a microcrack under residual and applied tensile stresses. That is, if the inclusion is too small to produce a microcrack during

cooling ($R < R_c^o$), then a microcrack can be produced at an applied stress (σ_a) dependent on the inclusion size:

$$R > R_c = R_c^o \, F \, (\frac{\sigma_a}{\sigma_r}) \quad ,$$

where the function $F\ (\sigma_a/\sigma_r)$ is < 1 and depends on the type of crack (e.g., circumferential or radial).

These results are important to the fabricator who must guard against strength degrading inclusions. The results tell the fabricator that despite the possibility of large residual stresses, inclusions will not produce any strength degradation at a given applied stress if their size is $< R_c$. These results are also important to those who would want to design new materials for new properties by producing composites of two (or more) compatible phases (e.g., to achieve a desired thermal expansion, etc.). That is, despite large differences in thermal and mechanical properties, two-phase composites can have mechanical integrity if the size of the second phase is less than a critical value.

Control of Grain Size

Bimodel and large grain size microstructures must be avoided to obtain high strengths. Large single grains within a fine grain matrix are common fracture origins. It is also well known that average strength is inversely proportional to the average grain size. Similar to the case of inclusions discussed above, localized stresses arise within and around grains due to thermal expansion and elastic anisotropy. The conditions for microcracking in single phase polycrystalline ceramics are similar to those of inclusions. That is, a critical grain size exist for spontaneous microcracking during cooling. Spontaneous microcracking occurs in single phase, polycrystalline Al_2O_3 with an average grain size $\gtrsim$ 80 μm. For materials exhibiting a much greater thermal expansion anisotropy, e.g., $MgTi_2O_5$[4] and Nb_2O_3,[5] the critical grain size is < 5 μm. Similar to the inclusion case, an applied stress will reduce the critical grain size required for spontaneous microcracking. Control of grain growth is therefore required for mechanical integrity.

It is well known that control of grain growth can be achieved with the addition of a chemically compatible second phase. As discussed in the previous section, two phase composites can be designed to avoid microcracking. Fig. 4 illustrates the strengthening that can be achieved for Al_2O_3 with additions of SiC with an average particle size of 4 μm.[6] Despite the large differential thermal expansion ($\alpha_{Al_2O_3} \simeq 8 \times 10^{-6}/^oC$, $\alpha_{SiC} = 4.2 \times 10^{-6}/^oC$), small additions (1 v/o to 8 v/o) of the 4 μm SiC can decrease the average grain size from ~ 30 μm to ~ 5 μm to increase the average strength by a factor of 1.6.

Recent results indicate that the second phase is most effective when located at 4-grain junctions, viz. it costs more energy to relocate the inclusion within a grain from a 4-grain junction than a 2-grain junction. Grain growth of the major phase will therefore be controlled by the number of 4-grain junctions filled by the second phase. Thus the second phase size distribution, volume fraction and uniformity of distribution are critical parameters. Fig. 5 illustrates the average Al_2O_3 grain size and the largest to average size ratio in various Al_2O_3/ZrO_2 composites as a function of temperature. At higher temperatures, grain growth control required ZrO_2 volume fractions > 0.075 for the given size distribution of starting powders. Note that 1 v/o ZrO_2 produces a much larger grain sizes relative to pure Al_2O_3. This result is caused by the non-uniformity of the ZrO_2 distribution, i.e., some portions of the material contained a higher concentration of ZrO_2 than others.

Kosmač et al[7] have shown the small additions of MgO (~ 1000 ppm) are also effective in further reducing the grains size in Al_2O_3/ZrO_2 composites.

It should be noted here that when colloid routes are employed to achieve a uniform phase distribution, the fabricator must guard against sedimentation. Figure 6 illustrates bottom and top regions of a slip cast β"-Al_2O_3/15 v/o ZrO_2 composite. The large ZrO_2 agglomerates and large β"-Al_2O_3 grains sedimented to the bottom. This problem can be avoided by pre-sedimentation as discussed above and/or by flocking the colloid prior to consolidation.

It can be concluded that the mechanical reliability of a ceramic can be increased by controlling grain growth with a dispersed second phase. This approach can be optimized with strict controls on phase distribution.

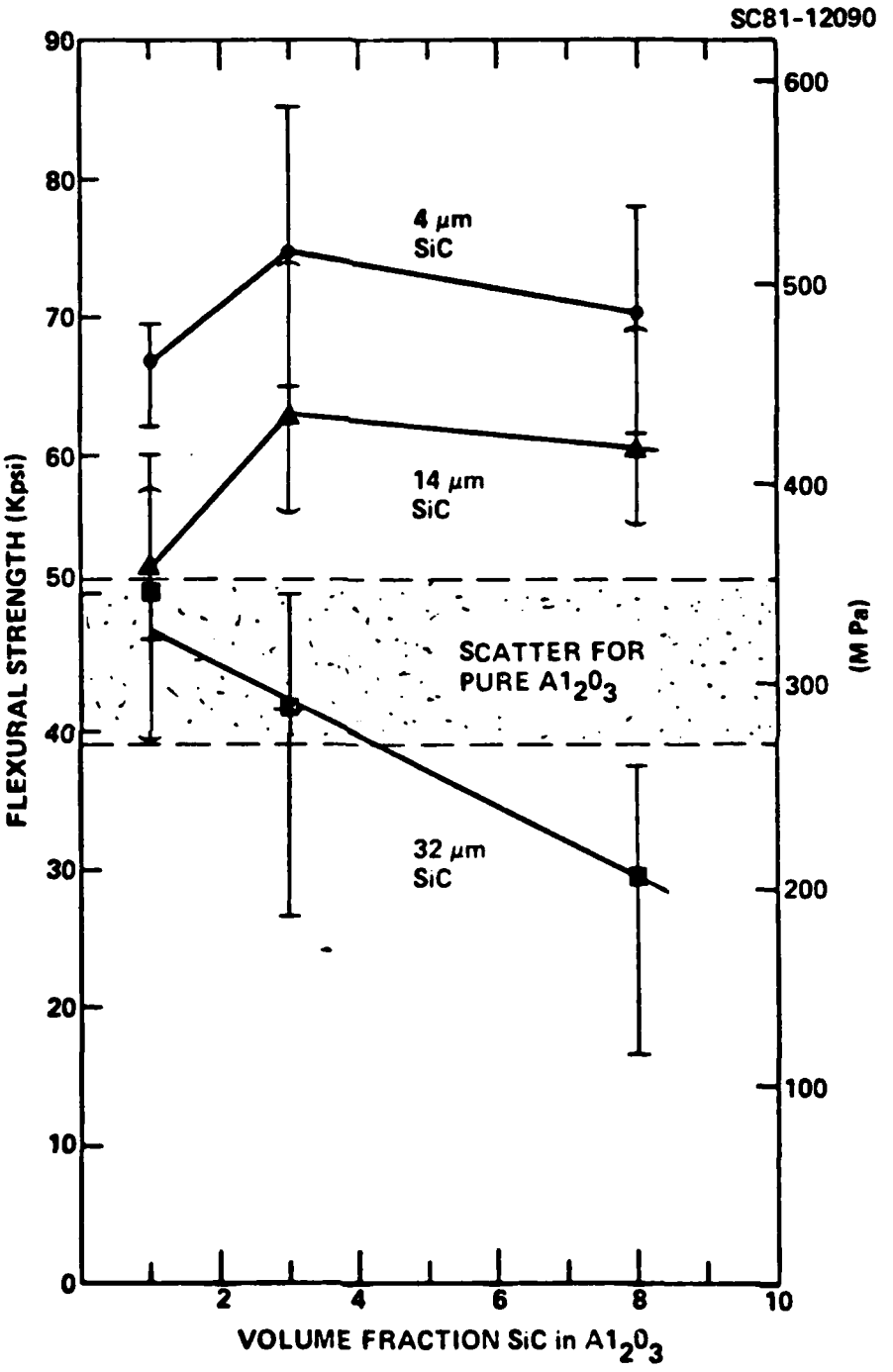

Fig. 4 Flexural strength of Al_2O_3/SiC composites vs volume fraction and size of SiC particulate.

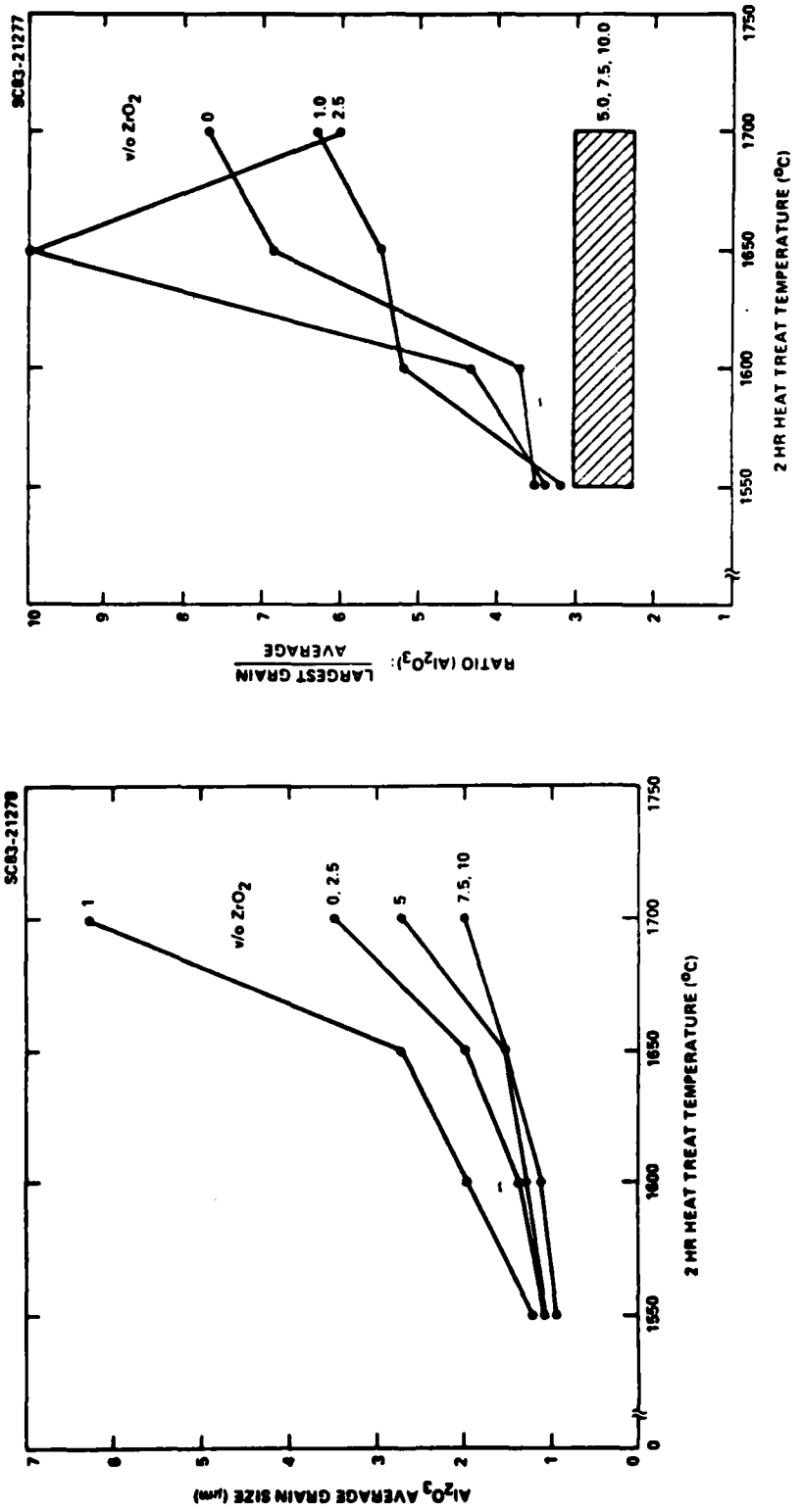

Fig. 5 Al_2O_3 average grain size (a) and ratio of largest to average size (b) for series of Al_2O_3/ZrO_2 composites vs heat treat temperatures (2 hrs).

SC83-21418 SC83-21419

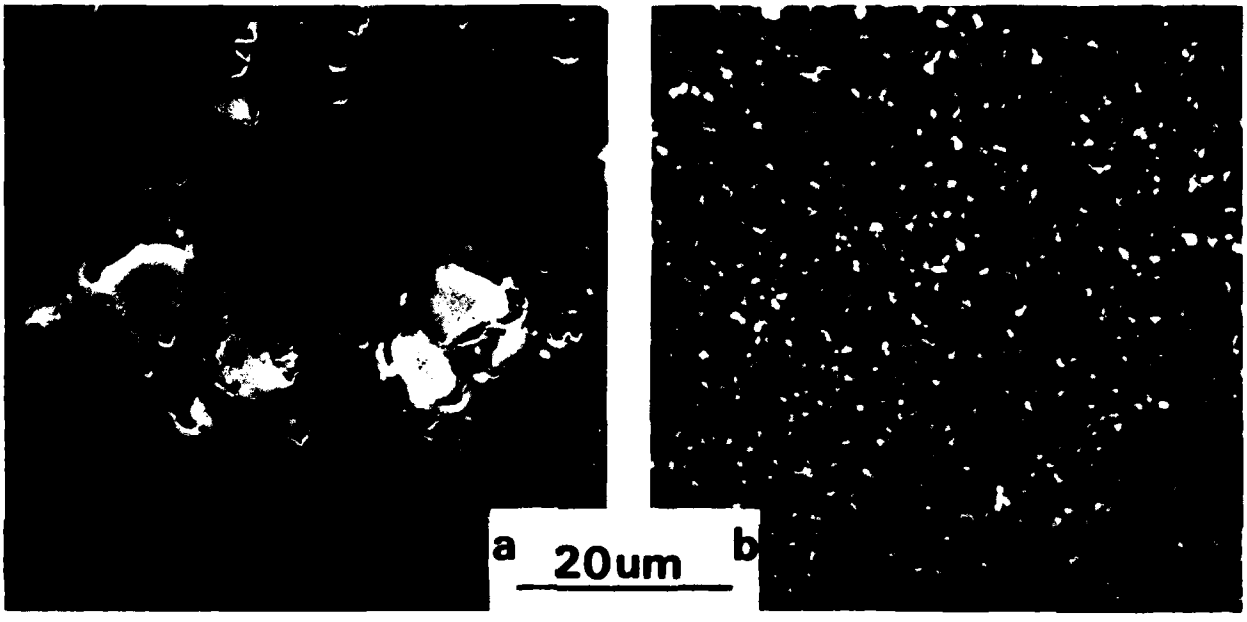

Fig. 6 Bottom (a) and top (b) regions of a filtered β"-Al_2O_3/ZrO_2 composite powder compact after sintering. Note large single phase areas on bottom due to sedimentation. (Courtesy of D.J. Green.)

3. Transformation Toughening (Rev. Ref. 8,9,10)

Of the various concepts that have been explored to increase the fracture toughness (K_c), transformation toughening has been most effective. Transformation toughening utilizes a rapid structural transformation that involves a molar volume increase and/or a shape change. Although this concept could be generally applicable to a variety of structural transformations, it has only been demonstrated for ZrO_2-based ceramics. Tetragonal ZrO_2 is the toughening agent. The increased toughness is derived from the work required to stress-induce the tetragonal to monoclinic ZrO_2 transformation in the vicinity of a propagating crack. Although tetragonal ZrO_2 appears to be more effective, monoclinic ZrO_2 can also be a toughening agent. In this case, material is fabricated to contain monoclinic ZrO_2 instead of tetragonal ZrO_2. For the monoclinic case, toughening is derived from the work required to produce and extend microcracks in the vicinity of a crack front. In materials that contain both tetragonal and monoclinic ZrO_2, both phenomena, i.e., stress induced transformation and microcracking can contribute to fracture toughness. As discussed elsewhere the amount of toughening derived from the tetragonal ZrO_2 depends on the t-ZrO_2 volume fraction and how close the transformation (constrained from occurring by its elastic surrounding) is from spontaneity. This condition depends on the thermodynamics of the constrain transformation, as governed by alloying additions to ZrO_2, ZrO_2 grain (or inclusion) size, elastic properties of the constraining matrix, temperature, etc.

In addition to the toughening phenomena just discussed, surface compressive stresses can be induced by surface grinding. Grinding induces the transformation only at the surface. The molar volume increase which accompanies the transformation places the surface in a state of compression. These surface compressive stresses can contribute as much to the strengthening as the increased fracture toughness. The magnitude and depth of the surface compressive stress appear to be controlled by the same parameters that control K_c.[11]

The following discussion will emphasize the fabrication requirements for retaining the tetragonal toughening agent.

A large particle of pure ZrO_2, unconstrained by any surrounding matrix, will usually undergo its t → m transformation upon cooling through ~ 1200°C. When the particle is placed within an elastic matrix and then cooled, the transformation temperature can be decreased to much lower temperatures, e.g., temperature approaching 0°K. As explained by classical theory, constraint lowers the transformation temperature because the strain energy, that would arise within and around the transforming volume, counters the free energy decrease due to the structural change. The elastic properties of the matrix and transforming inclusion and the transformation strain associated with the structural change are prime factors that govern the magnitude of the transformational strain energy. The structural free energy change is primarily governed by temperature and alloy additions. Thus, the constrained transformation will only be spontaneous at a temperature where the structural free energy decrease is greater than the strain energy increase. Retention of the high temperature tetragonal structure (i.e., the toughening agent) to room temperature (or lower) requires a constraining matrix with a high elastic modulus (which would increase the transformational strain energy) and, for some cases, alloying the ZrO_2 with another oxide (e.g., Y_2O_3), which decreases the structural free energy change at room temperature.

In all the ZrO_2 systems studied to date, it has been found that the retention of t-ZrO_2 also depends on its grain (or inclusion) size. That is, retention can only be achieved for sizes less than a critical size. This observation is not taught by classical thermodynamics and it is a current subject of theoretical controversy. Lange[12] argues that the size effect is caused by surface phenomena (microcracking and/or twinning) that accompany the transformation to reduce the transformation strain energy. The energy terms associated with these surface phenomena scale with the inclusion surface area, whereas the strain energy and structural free energy terms scale with the inclusions volume. This difference in scaling gives rise to a critical size effect. Evans,[13] who considered only the twinning surface effect, comes to the same conclusion through a different analytical approach. Heuer et al[14] believe the size effect is governed by nucleation. Regardless of the theory the reader chooses to accept, the critical size effect places strict microstructural constraints on the fabricator.

The ZrO_2-Y_2O_3 binary system[15] (Fig. 7) will be used to illustrate how 3 of the 4 basic microstructures that include the tetragonal ZrO_2 toughening agent are fabricated. Claussen[8] has shown how these microstructures can be combined to produce a larger variety. As shown, Y_2O_3 forms a solid solution with ZrO_2 ($Zr_{1-x}Y_xO_{2-x/2}$) to reduce the t → m transformation temperature from ~ 1200°C for pure ZrO_2 to ~ 600°C for the eutectoid composition containing ~ 3.5 m/o Y_2O_3.* Additions of > 7 m/o Y_2O_3 stabilize the cubic structure to room temperature.

One microstructure than can be produced is obtained by fabricating ZrO_2 containing ~ 3 to 7 m/o Y_2O_3 in the high temperature cubic phase field, and then quenching into the two-phase (tetragonal + cubic) field to precipitate tetragonal inclusions from the cubic matrix. If the inclusions do not grow to exceed a critical size, the two-phase material can be cooled to room temperature to retain the inclusions in their tetragonal structure. Such precipitated microstructures can be obtained in large single crystals by Scull melting, as demonstrated by Ingel et al,[16] and by sintering powders. The CSIRO Group (Garvie and Hannick[17]) have pioneered this sintered microstructure in the ZrO_2-CaO system, and the Case-Western Group (Heuer and students)[18] in the ZrO_2-MgO system. The sintered microstructures consist of large cubic grains (a result of high temperatures sintering) which contain the internal and grain boundary tetragonal precipitates. The volume fraction of the precipitates is governed by the alloying agent and the heat treatment schedule in the two-phase field.

A second microstructure, consisting of polycrystalline, single phase tetragonal ZrO_2, can be fabricated by sintering composite ZrO_2 + Y_2O_3 (< 3 m/o) powders in the tetragonal phase field, provided that the resulting grain size is less than the critical value (dependent on the Y_2O_3 content). Gupta et al,[19] pioneered this microstructure. Here, neighboring grains constrain one another from the anisotropic transformation strains.

*m/o = mole %; v/o = volume %.

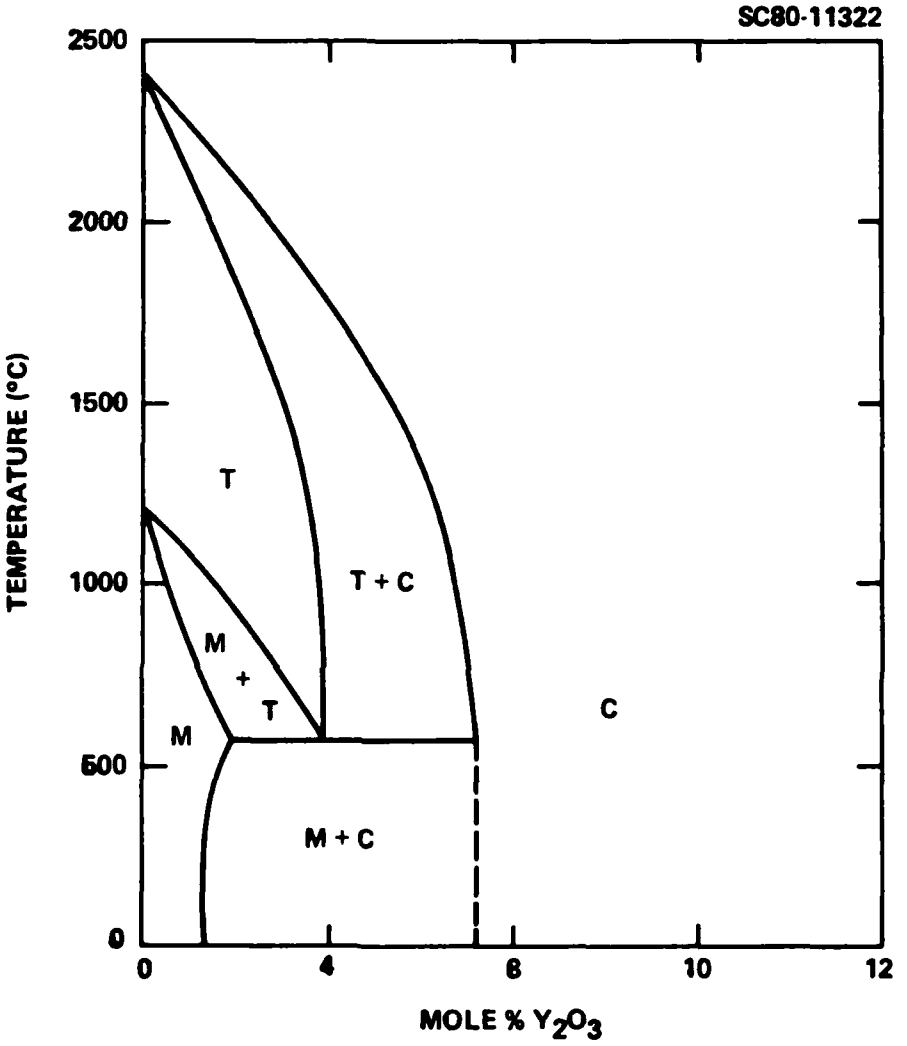

Fig. 7 Portion of the ZrO_2-Y_2O_3 binary.

The third microstructure, pioneered by Lange,[12] is a two-phase, tetragonal/cubic polycrystalline material in which neighboring grains are either tetragonal or cubic. This microstructure is fabricated by sintering ZrO_2 + Y_2O_3 composite powders in the two-phase, t + c field. Here again, the tetragonal phase is retained only if the fabricated grain size does not exceed a critical value. The volume content of the tetragonal phase can be varied from 100% to 0% by changing the Y_2O_3 content from ~ 3 m/o to ~ 7 m/o.

The fourth microstructure is developed by incorporating ZrO_2 into a chemically compatible matrix phase to obtain a polycrystalline, two-phase material by sintering. The Al_2O_3/ZrO_2 composite system, pioneered by Claussen,[20] is typical of such systems. Except for very dilute composites (< 10 v/o of the minor phase) on either end of the binary, the composite is itself the constraining matrix. Here, as with other two-phase ceramics, the volume fraction at which the minor phase becomes continuous depends on the dihedral angle. Although the minor phase is primarily located at three and four grain junctions, smaller second phase grains can be observed within the major phase grains indicative of entrapment during grain growth.

As indicated, retention of the t-ZrO_2 toughening agent requires strict microstructural control to achieve a high density ceramic (required for constraint) and a ZrO_2 grain (inclusion) size < 1 μm (depending on elastic constraint and alloying addition).[12,21] For fabrication routes involving precipitation, once the particular composition has been selected, microstructural controls are primarily exerted after densification, i.e., during cooling to the two-phase region and aging. For other routes that involve powders, microstructural control starts with the powder. It is obvious that if the critical grain size is < 1 μm, the size distribution of the crystallites in the powder must be much smaller. Powders with crystallite sizes in the range of 0.1 μm are derived by decomposition reactions, e.g., from $ZrOCl_2$; such powders can contain a large fraction of hard agglomerates. These agglomerates not only produce crack-like voids during sintering, they also result in an inhomogeneous phase distribution, lead to exaggerated grain growth and hinder sintering kinetics.

A major problem concerning powder routes is that since grain growth is concurrent with densification, and both phenomena are controlled by temperature and time, it can be difficult (or experimentally impossible) to achieve > 0.98 ρ_t without grains exceeding their critical size. For example, theory suggests that pure, polycrystalline ZrO_2 can be fabricated as single phase, t-ZrO_2. But, unfortunately, the critical grain size is ~ 0.02 μm, which would impose extreme fabrication constraints. Alloying additions of 2 m/o Y_2O_3 increase the critical grain size to ~ 0.2 μm, which can be fabricated with some difficulty, whereas 3 m/o Y_2O_3 increases the critical grain size to 1 μm which is easily achieved with current powders.[12] Thus alloy additions which decrease the transformational free energy aid the fabricator in retaining t - ZrO_2 within the present day constraints on fabrication.

4. Concluding Remarks

Transformation toughening, as demonstrated with the tetragonal-ZrO_2 toughening agent, offers great potential for developing ceramics with significant tensile strengths. Retention of the toughening agent, e.g., tetragonal ZrO_2, requires strict processing controls to achieve a dense ceramic with a grain (inclusion) size less than a critical value. With the exception of the precipitated microstructure, the grain size restriction requires sub-micron powders. Alloy additions (e.g., Y_2O_3), which can be best accomplished during powder manufacture, are necessary for single phase polycrystalline ZrO_2 and many composite microstructures. The alloy addition increases the critical grain size to allow for some grain growth during densification without exceeding the critical size. As discussed elsewhere, once one retains the tetragonal phase, fracture toughness is optimized by a) increasing the t-ZrO_2 volume fraction, 2) increasing the composite modulus, 3) decreasing the alloy addition (sufficient to still retain the tetragonal phase), and 4) achieving a grain (inclusion) size just less than critical.

The potential offered by transformation toughening to increase strength depends on processing which governs the flaw size distribution and microstruc-

tural uniformity. Agglomerates appear to be the greatest culprits by producing the largest strength degrading flaws for processing that involves pressureless sintering. Powders free of hard agglomerates and colloidal processing routes appear to be required to avoid either hot-pressing or HIPping, both of which help close the crack-like voids produced by the agglomerates. Thus, great gains are expected from improved processing with both transformation toughened and other ceramics.

References

1. F.F. Lange, M. Metcalf, B.I. Davis and I.A. Aksay, "Processing Related Fracture Origins: Parts 1, 2, 3," J. Am. Ceram. Soc. (in press).

2. I.A. Aksay, B.I. Davis and F.F. Lange, J. Am. Ceram. Soc. (in press).

3. D.J. Green, "Microcracking Mechanisms in Ceramics," Fracture Mech. of Ceramics Vol. 5, 457, ed. by R.C. Bradt, D.P.H. Hassleman, F.F. Lange and A.G. Evans, Plenum Press (1983).

4. J.A. Kuszyk and R.C. Bradt, J. Am. Ceram. Soc. 56, 420 (1973).

5. W.R. Manning, O. Hunter, Jr., F.W. Calderwood, and D.W. Stacy, J. Am. Ceram. Soc. 55, 342 (1972).

6. F.F. Lange, unpublished.

7. T. Kosmač, J.S. Wallace and N. Claussen, J. Am. Ceram. Soc. 65, C-66 (1982).

8. N. Claussen, "Transformation-Toughened Ceramics," European Colloquium on Ceramics in Advanced Energy Technologies, Sept. 20-22, 1982, Petten, The Netherlands (in press).

9. F.F. Lange, "Transformation Toughening: A Thermodynamic Approach to Phase Retention and Toughening," ibid (Ref. 3) Vol. 6.

10. First International Conference on the Science and Technology of Zirconia, Advances in Ceramics, Vol. 3, The American Ceramic Society, 1981.

11. D.J. Green, F.F. Lange and M.R. James, "Factors Influencing the Residual Surface Stresses Due to a Stress-Induced Phase Transformation," submitted to J. Am. Ceram. Soc.

12. F.F. Lange, J. Mat. Sci. 17, 225 (1982).

13. A.G. Evans, N. Burlingame, M. Drory, W.M. Kriven, Acta Met. 29, 447 (1981).

14. A.H. Heuer, N. Claussen, W.M. Kriven and M. Rühle , J. Am. Ceram. Soc. 65, 642 (1982).

15. K.K. Srivastava, R.N. Patil, C.B. Chandary, K.V.G.K. Gokhale and E.C. Subbarao, Trans. Brit. Ceram. Soc. 73, 85 (1974).

16. R.P. Ingel, R.W. Rice and D. Lewis III, J. Amer. Ceram. Soc. 65, C108 (1982).

17. R.C. Garvie, R.H. Hannick and R.T. Pascoe, Nature 258, 703 (1975).

18. D.L. Porter and A.H. Heuer, J. Am. Ceram. Soc., 60, 280 (1977).

19. T.K. Gupta, F.F. Lange and J.H. Bechtold, J. Mat. Sci 13, 1464 (1978).

20. N. Claussen, J. Am. Ceram. Soc. 59, 49 (1976).

21. D.J. Green, J. Am. Ceram. Soc. 65, 610 (1982).

APPENDIX IV

HINDRANCE OF GRAIN GROWN IN Al_2O_3 by ZrO_2 INCLUSIONS

Rockwell International
Science Center

SC5295.2AR

HINDRANCE OF GRAIN GROWTH IN Al_2O_3 by ZrO_2 INCLUSIONS

F.F. Lange and M. Hirlinger

Structural Ceramics
Rockwell International Science Center
Thousand Oaks, CA 91360

ABSTRACT

Alumina and Al_2O_3/ZrO_2 (1 to 10 volume %) composite powders were mixed and consolidated by a colloidal method, sintered to > 98% theoretical density at 1550°C, and were then subsequently heat treated at temperatures up to 1700°C for grain sizes measurements. Within the temperature range studied, the ZrO_2 inclusions exhibited sufficient self diffusion to move with the Al_2O_3 4-grain junctions during grain growth. Growth of the ZrO_2 inclusions occurred by coalescence. The inclusions exerted a dragging force at the 4-grain junctions to limit grain growth. Abnormal grain growth occurred when the inclusion distribution was not sufficiently uniform to hinder the growth of all Al_2O_3 grains. This condition was observed for compositions containing < 2.5 v/o ZrO_2. Exaggerated grains would consume both neighboring grains and ZrO_2 inclusions. Grain growth control (no abnormal grain growth) was achieved when a majority (or all) 4-grain junctions contained a ZrO_2 inclusion, viz for compositions containing > 5 v/o ZrO_2. For this condition the grain size was inversely proportional to the volume fraction of the inclusions. Since the ZrO_2 inclusions mimic voids in all ways except to disappear, it is hypothesized that abnormal grain growth in single phase materials is a result of a nonuniform distribution of voids during the last stage of sintering.

1. INTRODUCTION

Grain growth inhibition is desirable for preventing abnormal grain growth during sintering, which swallow pores to limit end-point densities, and for limiting grain size to achieve higher strengths.* Second phase inclusions can inhibit grain growth and are frequently used for this purpose in metal systems. Although most high performance ceramics are not single phase materials, the use of a particular second phase to inhibit grain growth is not currently practiced due to the common belief that inclusions are precursors to strength degrading microcracks. Although inclusions can produce microcracks, theoretical work has shown that despite the high residual stresses developed by differential thermal expansion (or phase changes), microcracking can be avoided both during cooling from the fabrication temperature and during subsequent stressing if the inclusion size is less than a critical value.[1,2] This theoretical work has opened the realm of designing two (or more) phase systems without the worry of degrading strength and other properties related to microcracking. This has been recently demonstrated for Al_2O_3/SiC composites.[3] Despite the large differential thermal expansion (the thermal expansion of Al_2O_3 is twice that of SiC), a SiC dispersed phase inhibits grain growth to produce a 65% strength increase relative to polycrystalline Al_2O_3 fabricated under identical conditions.

Theory that treats the inhibition of grain growth by inclusions has been generally based on refinements of Zener's[4] original concept in which the inclusion residing at grain boundaries, produces a dragging force, due to the lower free energy of the junction/inclusion system when the inclusion resides at the junction. Ashby and Centamore[5] have shown that the inclusion(s) can move with the junction if the inclusion exhibits sufficient self diffusion. Theory suggests that the velocity of the moving inclusion (v_i) will depend on its radius r as either r^{-3} or r^{-4}, for interfacial diffusion or volume diffusion, respectively.[6]

*Each grain can be considered a precursor to a microcrack due to either residual stresses arising from thermal expansion anisotropy or effects of surface machining.

In metal systems, inclusions are commonly introduced by precipitation, internal oxidation, mechanical alloying, etc. and they are usually used to control grain growth during the recrystallization that precedes deformation at temperatures where the inclusions velocity is nearly zero. These methods of introducing inclusions into ceramics are ineffective since grain growth inhibition must be concurrent with sintering. Thus, inclusions must be introduced as a second phase particulate dispersion into the major phase powder prior to sintering. Since detailed studies of inclusion/grain-junction interactions have not been detailed for this method of fabrication, studies were initiated by investigating the effect of ZrO_2 additions on the grain growth phenomena of Al_2O_3. This system was not only chosen for its technical interest as a transformation toughened material for which Green[7] has already phenomenally characterized grain growth to determine critical ZrO_2 inclusion size required to retain the tetragonal structure, but also for the large difference in atomic number between Al and Zr, which results in high contrast between the two chemically compatible phase when examined with electron microscopy. Also, since powders of both phase can be sintered within the same temperature range (1300°C to 1600°C), it was suspected that sufficient self diffusion would exist within the ZrO_2 to permit analogies with pore/grain boundary interactions.

2.0 EXPERIMENTAL

α-Al_2O_3 and cubic-ZrO_2 (+6.6 mole % Y_2O_3) powders were separately dispersed in distilled water containing HCl to maintain a pH of 2 to 3 for periods of up to 24 hr.* Each powder was sedimented to collect all particles < 1 μm. The supernate containing < 1 μm particles was immediately flocced by increasing the pH to 8 with additions of NH_4OH. Flocculation consolidated the dispersion to volume % of ~ 16 and ~ 5 for the sedimented Al_2O_3 and ZrO_2 powders, respectively, and prevent mass segregation during storage. The small salt content resulting from pH controls was minimized by mixing the flocced slurries with deionized water followed by spontaneous floccing. The solid contents of each

*Initial reactions of the powders with pH = 2 water tended to increase the pH which decreased the stability of the dispersion.

flocced slurry was determined by density measurements and the assumed density of each phase ($\rho_{Al_2O_3}$ = 3.98 gm/cc, ρ_{ZrO_2} (cubic) = 6.03 gm/cc). Figure 1 illustrates the size distribution of the two powders after they were redispersed at pH = 2, diluted to ~ 2 volume % and ultrasonically treated.

Two phase flocced slurries containing 0, 1.0, 2.5, 5.0, 7.5 and 10.0 volume % ZrO_2 were prepared by weighing the appropriate amounts of each slurry, redispersing each at pH = 2 with HCl, mixing together with ultrasonic treatment and again flocculating at pH = 8 with NH_4OH. As described elsewhere, consolidation was performed by centrifuging at ~ 2000 times gravity. The centrifuged, plastic mass was dried and cut into specimens and sintered together at 1550°C for 1 hr.* All materials had a sintered density > 97% of theoretical based on the theoretical densities of the two phases.

Each material was diamond cut into a smaller specimen and one surface was highly polished. Thermal etching was performed at 1550°C for 1 hr. Polished, thermal etched surfaces were observed in the scanning electron microscope using a combined backscattering and secondary electron collecting mode to enhance the contrast between the two phases required to measure the size distribution of the brighter ZrO_2 inclusions.

A number (4 to 8) of micrographs were taken at a magnification for which every Al_2O_3 grain could be analyzed with an image analyzer. The size distribution of the Al_2O_3 grains were obtained by tracing the grain boundaries on the micrographs with black ink on a transparent overlay which was suitable for image analyzing. The image analyzer was programmed to convert each phase area into an equivalent circle to obtain its equivalent diameter. These data were reduced to a histogram and pertinent statistical parameters. The same specimens were then heat treated for two hours at 1600°C, 1650°C, and 1700°C. Specimens containing 1, 5, 7.5 and 10 volume % ZrO_2 were also heat treated at 1650°C for 2 hr, 6 hr and 12 hr prior to the 1700°C heat treatment. After each heat treatment, the size distribution of both the ZrO_2 and Al_2O_3 grains were

*Initial sintering experiments showed that a sintering temperature of 1525°C (1 hr) produced densities < 95% of theoretical.

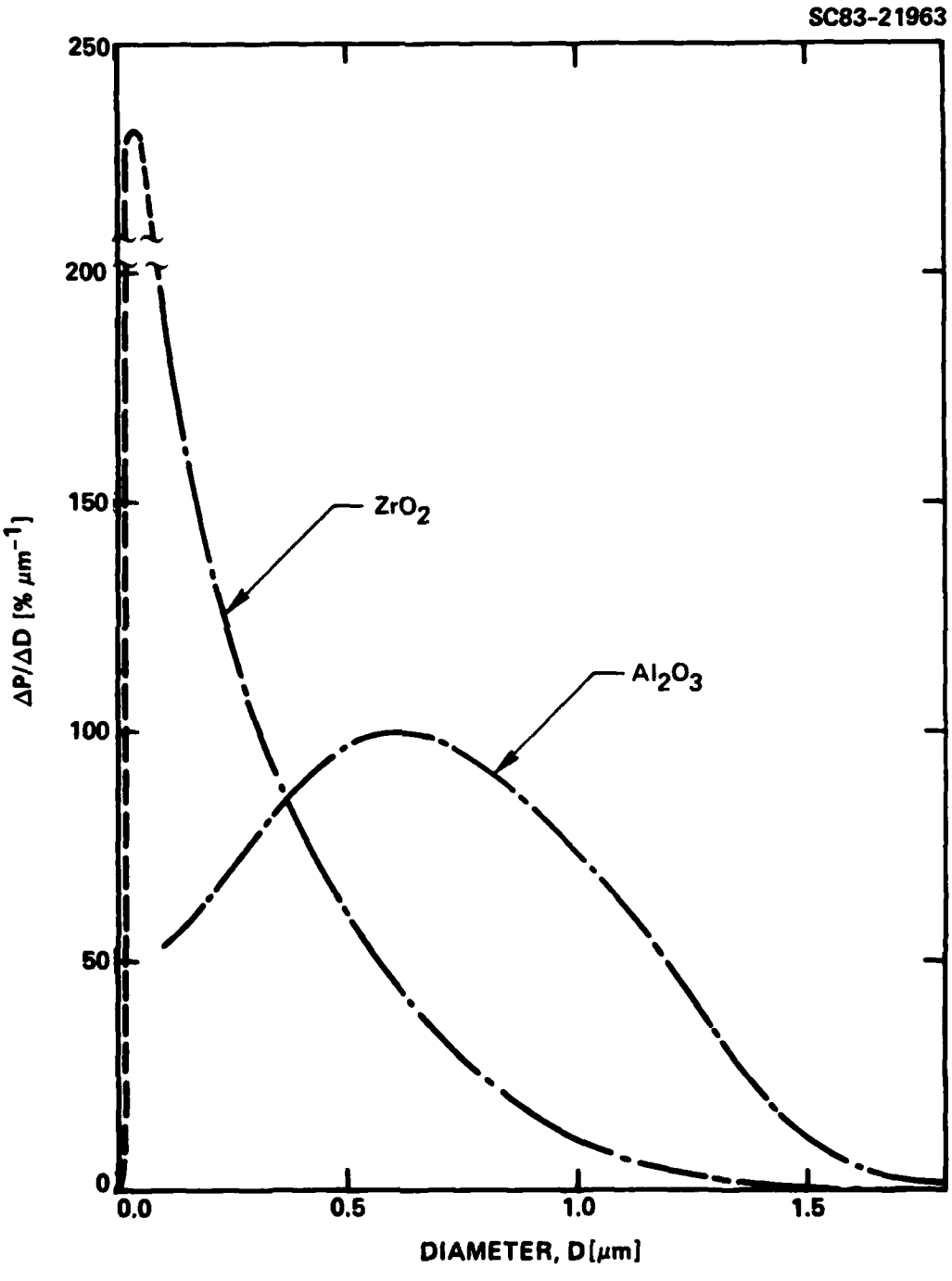

Fig. 1 Size distribution of the colloidally treated Al_2O_3 and ZrO_2 powders.

obtained by the same procedure discussed above. The number of grains observed for each phase was dependent on the volume fraction of the ZrO_2 and the development of a bimodal distribution for the Al_2O_3. Different magnifications were used for bimodal microstructures.

In addition, separate specimens containing 1 and 7.5 volume % ZrO_2 were directly sintered at 1700°C for 2 hr without the intermediate heat treatments.

3. RESULTS

3.1 Grain Growth Data

Table 1 lists the statistical information reported as mean grain size of the Al_2O_3 (A) and ZrO_2 (Z), mean size ratio of the two phases (Z/A), and the largest to mean size ratio of the Al_2O_3 phase (AR). Values of AR indicated the bimodal nature of the microstructure. The determination of AR was somewhat subjective for extreme bimodal microstructures since it was uncertain that the largest grain was photographed during examination. Figure 2 illustrates the mean grain size of the Al_2O_3 (a) and the largest to mean ratio (b) as a function of the 2 hr, heat treatment temperatures.

Figure 2a shows that the mean Al_2O_3 grain size is not a monotonic function of the ZrO_2 content, viz. the grain size for composites with 1 v/o and 2.5 v/o ZrO_2 were greater and equal to that for the single phase Al_2O_3, respectively. Figure 2b shows that all of the materials containing < 2.5 v/o were strongly bimodal at temperatures > 1600°C, whereas grain growth control (normal grain growth) was achieved for ZrO_2 contents > 5 v/o.

Table 1 shows that the mean size of the ZrO_2 inclusions at 1550°C are larger than the mean size in the initial ZrO_2 powder and that they further grow during heat treatments at temperatures > 1550°C. In general, their size after a given heat treatment increase with ZrO_2 volume fraction. Analysis of the growth of the ZrO_2 inclusions as a function of time at 1650°C did not correlate with any theory concerning Ostwald ripening.

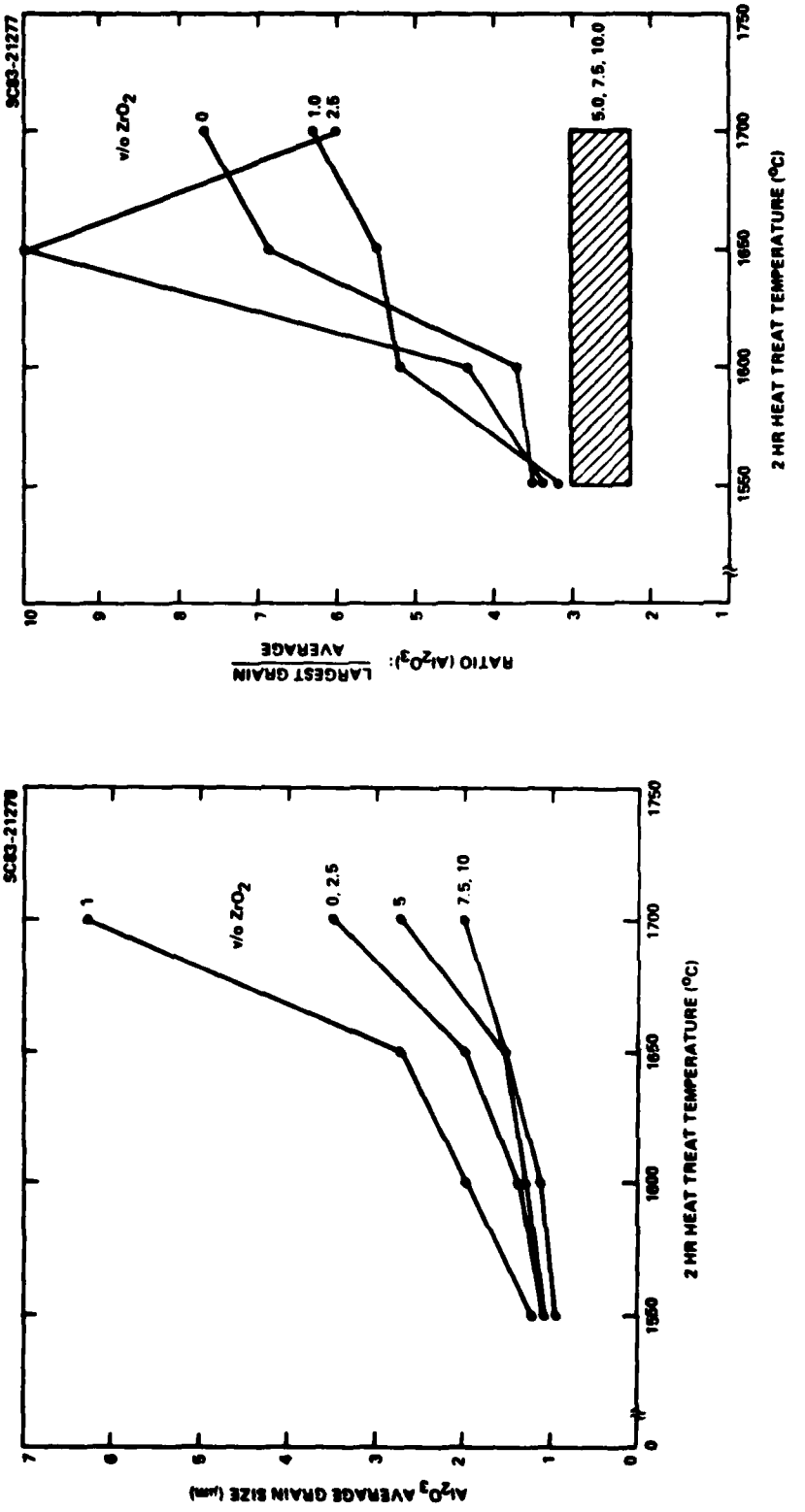

Fig. 2 a) Mean Al_2O_3 grain size vs heat treatment temperature (2 hr)
b) Ratio of largest to mean Al_2O_3 grain size vs heat treatment temperature (2 hr).

Table 1

Grain Size Data for Al_2O_3 and Al_2O_3/ZrO_2 Composites

v/o ZrO_2		Heat Treatment Temperature (Time) °C (hr) 1550 (2)	1600 (2)	1650 (2)	1605 (6)	1650 (12)	1700 (2)	1700* (2)
0	A	1.09	1.36	1.95	-	-	3.52	3.74
	AR	3.5	3.7	6.9	-	-	7.7	4.0
1	A	1.21	1.98	2.69	3.74	5.28	6.30	11.50
	Z	0.54	0.55	-	-	-	-	-
	AR	3.2	5.2	5.5	6.4	6.4	6.3	3.5
	Z/A	0.45	0.27	-	-	-	-	-
2.5	A	1.05	1.31	2.04	-	-	3.48	-
	Z	0.44	0.54	-	-	-	-	-
	AR	3.4	4.4	10.0	-	-	6.0	-
	Z/A	0.41	0.41	-	-	-	-	-
5	A	1.05	1.23	1.49	1.98	2.48	2.75	-
	Z	0.52	0.58	0.65	0.84	0.96	1.32	-
	AR	2.66	2.92	2.82	3.13	3.50	2.76	-
	Z/A	0.37	0.47	0.43	0.42	0.39	0.48	-
7.5	A	0.95	1.32	1.57	1.73	1.95	2.01	2.08
	Z	0.51	0.72	0.93	0.89	0.94	1.19	-
	AR	2.75	3.03	2.48	2.54	2.90	2.69	3.17
	Z/A	0.54	0.54	0.59	0.52	0.48	0.59	-
10	A	0.91	1.09	1.48	1.51	1.91	1.90	-
	Z	0.57	0.74	0.98	0.97	1.21	1.20	-
	AR	3.07	3.02	2.84	2.78	3.03	2.21	-
	Z/A	0.63	0.68	0.66	0.64	0.63	0.63	-

*Specimens heated directly to 1700°C/2 hr.

A = Al_2O_3 mean size (μm)

Z = ZrO_2 mean size (μm)

AR = Largest Al_2O_3 grain/mean size

Z/A = Mean ZrO_2/mean Al_2O_3.

For composites exhibiting controlled grain growth (> 5 v/o ZrO_2) the mean size ratio of the two phases (Z/A) was nearly constant at all temperatures and increased with the ZrO_2 volume fraction (see Table 1).

Direct heating of the 7.5 v/o ZrO_2 composition to 1700°C/2 hr produced a nearly identical microstructure relative to the same material sintered at 1550°C and sequentially heated to 1700°C (see Table 1). This was not the case for the Al_2O_3 without a dispersed phase and the 1 v/o ZrO_2 composition. Direct heating to 1700°C/2 hr produced a larger grain size without the severe bimodal characteristics relative to the same materials heated sequentially to 1700°C. These observations suggest that the conditions for exaggerated grain growth are history dependent and may reflect a nucleation/growth phenomenon for abnormal grain growth.

3.2 Microstructures

For composites exhibiting controlled grain growth (> 5 v/o ZrO_2), fracture surface observations showed that the ZrO_2 grains were primarily located at 4-grain junctions as illustrated in Fig. 3 for the case of 7.5 v/o ZrO_2 heated to 1700°C/2 hr. (Surface observations used to determine grain size limits observations to apparent 3-grain junctions.) It is obvious that ZrO_2 particles, initially located between the Al_2O_3 particles were sufficiently mobile during growth of the Al_2O_3 grains to remain located at 4-grain junctions. That is, growth of the ZrO_2 grains occurred by coalescence as depicted in Fig. 4a; Fig. 4b illustrates that ZrO_2/ZrO_2 grain boundaries were frequently observed, indicative of a coalesence mode of growth.

For compositions that produced a bimodal Al_2O_3 grain size distribution (< 2.5 v/o ZrO_2), the ZrO_2 grains were primarily located at 4-grain junctions only at 1550°C. At higher temperatures more and more ZrO_2 grains became relocated within the interior of the Al_2O_3 grains and had a spherical geometry. This phenomena appeared to occur by the growth of a group of Al_2O_3 grains contained by relatively few ZrO_2 grains, into a large grain which then swallowed up surrounding Al_2O_3 and ZrO_2 grains. As shown in Fig. 5, the Al_2O_3 grains in local regions with a greater ZrO_2 concentration, remained small until they were

SC83-22460

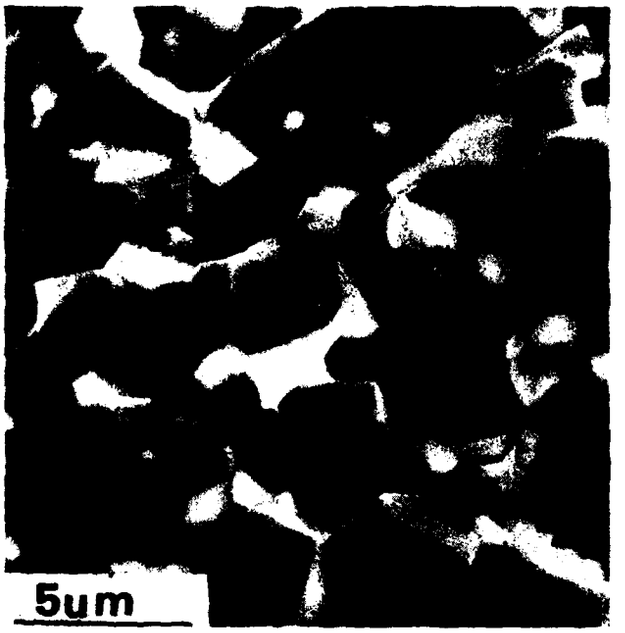

Fig. 3 Fracture surface of 7.5 v/o ZrO_2 composition after heat treatment at 1700°C/2 hr. Note most of ZrO_2 inclusions are at 4-grain junctions.

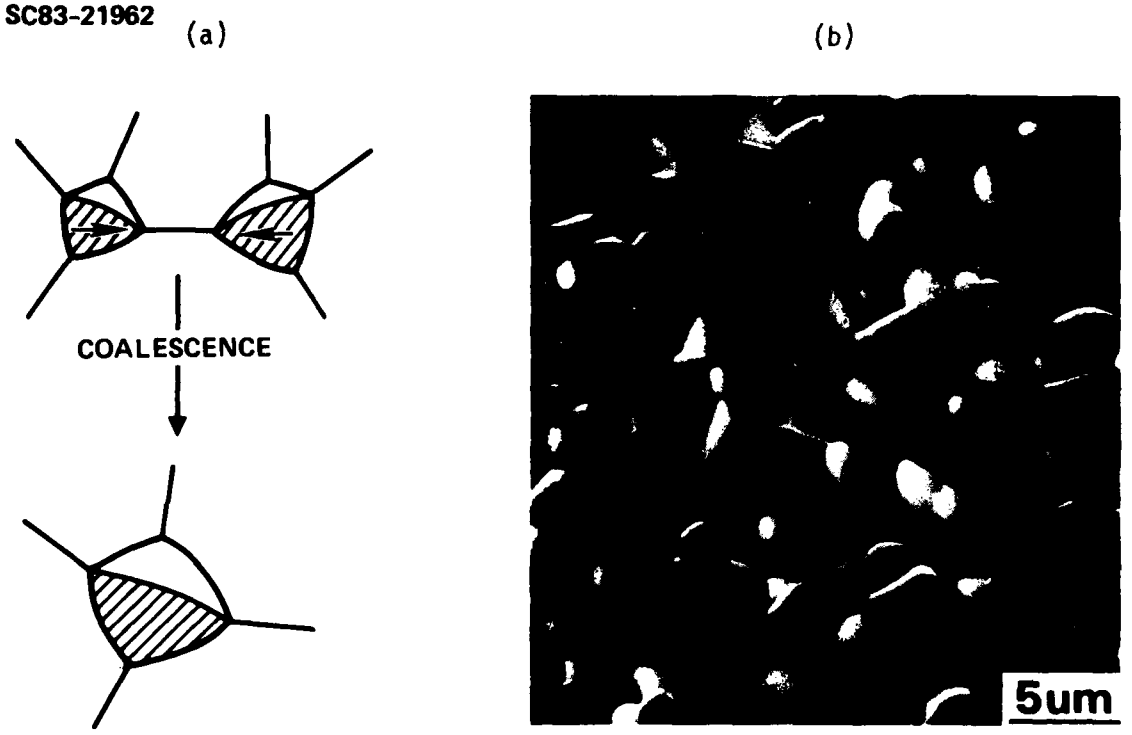

Fig. 4 a) Coalescence of inclusions at 4-grain junctions, b) observations of several ZrO_2 grains at 4-grain junctions resulting from coalescence (5 v/o ZrO_2, 1700°C/2 hr).

SC83-22461

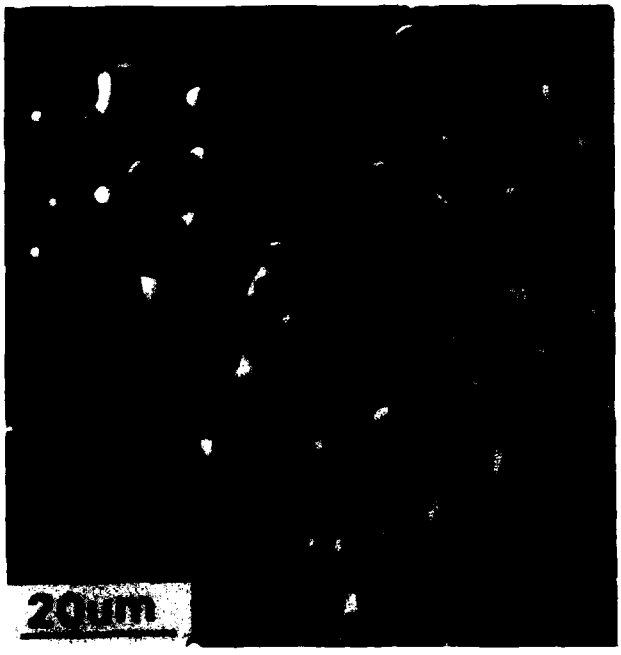

Fig. 5 Regions of small Al_2O_3 grains constrained by ZrO_2 inclusion surrounded by large, exaggerated grains. Note arrow-head shape of inclusions at 3- (or 4-) grain junctions.

engulfed by much larger, surrounding grains. That is, abnormal grain growth appeared to be promoted by the nonuniform distribution of the ZrO_2.

Within regions only containing abnormally large Al_2O_3 grains, the ZrO_2 grains were > 10 times smaller than the Al_2O_3 grains. At two-grain junctions the ZrO_2 grains were observed in various drag/break-away configurations as shown in Fig. 6a; Fig. 6b shows the rare configuration of imminent break-away. Measurement of the dihedral angle (ψ) with symmetric ZrO_2 grains located at 2-grain junctions resulted in $\psi = 80° \pm 5°$. This suggests that the Al_2O_3/ZrO_2 interfacial energy is $\approx 2/3$ the Al_2O_3 grain boundary energy.

The arrow-head shape of ZrO_2 grains at 3-grain junctions (or, possibly 4-grain junctions) also indicates a condition of inclusion drag as recently pointed out by Evans[8,9] and coworkers for the case of a pore being dragged by a 3-grain junction (see Fig. 7a.) Examples of these shapes are shown in Fig. 5. Figure 7b schematically shows three configurations observed for inclusion close to a 3-grain junction. These shapes suggest that the inclusion has recently broken away from the 3-grain junction, by either the movement of two grain boundaries (configuration 1) or by the movement of any one of the grain boundaries (configuration 2 and 3).

4. DISCUSSION

4.1 Grain Growth Control

The grain growth data and direct observations showed that the self diffusion of ZrO_2 was sufficient at all temperatures to allow the ZrO_2 inclusions, initially located between Al_2O_3 particles in the composite powder, to locate and remain at 4-grain junctions as grains grew during sintering. During sintering, i.e., temperatures up to 1550°C, the ZrO_2 grains had only a small effect on grain growth kinetics, viz, 10 v/o ZrO_2 only reduced the grain size relative to the Al_2O_3 without a dispersed phase by ~ 20% at 1550°C.

At higher temperatures, the ZrO_2 inclusions still had only a small effect (20 to 30%) on grain size for compositions (> 5 v/o ZrO_2) exhibiting controlled grain growth. Evans and coworkers[9] has shown that the grain growth

SC83-22462

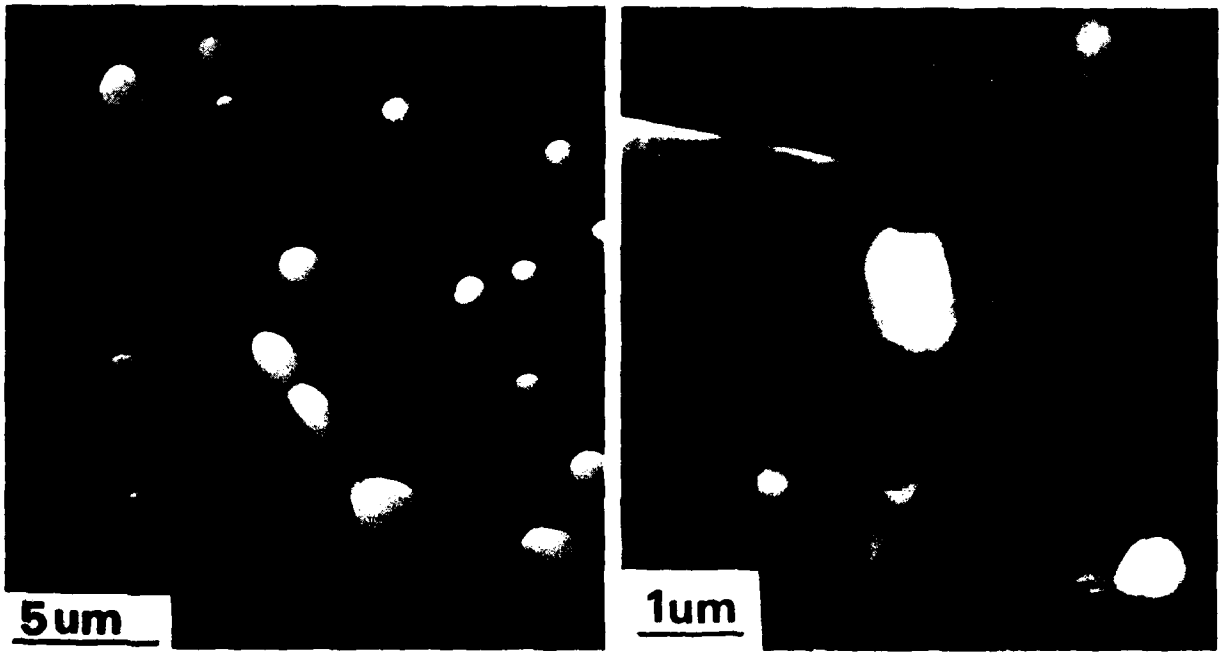

(a) (b)

Fig. 6 a) Drag configuration of ZrO_2 inclusions at 2-grain junction and b) imminent break-away configuration.

SC83-21961

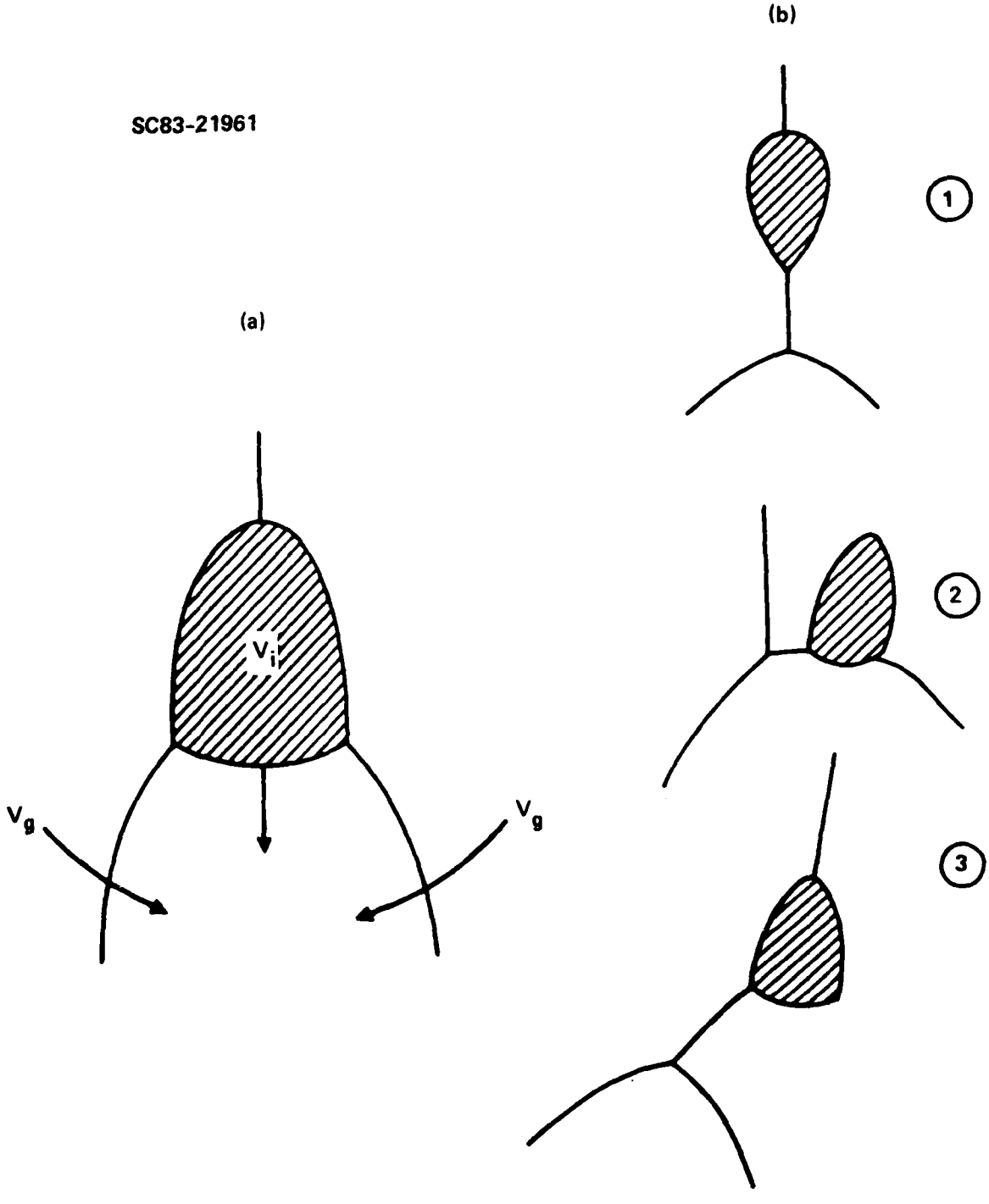

Fig. 7 a) Arrow-head shape of an inclusion being dragged along with a 3-grain junction (after Evans), b) observed break-away configurations.

hindrance exerted by pores located at 3-grain junctions is directly proportional to the pore size to grain size ratio. The same theoretical arguments would also apply to 4-grain junctions. Inclusions that exhibit sufficient self diffusion will behave as pores. As shown in Table 1, the inclusion size to grain size ratio (Z/A) remains constant for compositions exhibiting controlled grain growth due to coalescence and this ratio increases with increasing ZrO_2 volume fraction. For these compositions, the hindrance to grain growth is directly proportional to Z/A and therefore related directly to the volume fraction of ZrO_2.

The major effect of the ZrO_2 inclusions was in preventing abnormal grain growth. All evidence suggests that abnormal grain growth was promoted by the rapid growth of a small group of grains to form a large grain, which in turn, rapidly swallowed neighboring grains and inclusions. Observations (see Fig. 5) strongly suggest that a nonuniform distribution of the ZrO_2 inclusions will promote exaggerated grain growth. Also note the much larger grain sizes of the composition containing 1 v/o ZrO_2 compared to the Al_2O_3 without the dispersed phase. Namely, groups of grains not containing inclusions grew rapidly, whereas neighboring grains hindered by ZrO_2 did not. It can be hypothesized that controlled grain growth will be achieved when most 4-grain junctions are filled with an inclusion. It can thus be postulated that for a given size distribution of the inclusion phase, grain growth control can be achieved for an inclusion volume fraction that fills all 4-grain junctions. The volume fraction required to meet this criterion will decrease with the mean size of the inclusion phase.

4.2 Analogies to Pore/Grain Size Phenomena

If the dominating path of ZrO_2 diffusion is at the ZrO_2/Al_2O_3 interface, theory indicates that inclusions will mimic the behavior of pores in all ways except one, viz, pores can disappear by mass transport (i.e., the phenomena of sintering), whereas inclusion cannot. Analogies between pores and inclusion have already been presented above concerning drag and break-away configurations. Of greater interest here is the analogies concerning pore volume change and grain growth, and conditions leading to abnormal grain growth.

Recent observations have shown that sintering is not a homogeneous process, viz, small regions reach full density prior to the bulk. These dense regions support grain growth. The pores separating the dense regions prevent abnormal grain growth, i.e., grain growth is confined to the dense regions. As these pores shrink and disappear, one can classify the pore/grain growth phenomena with two extreme cases. The first case is where grain growth kinetics is greater than the kinetics for pore disappearance. The second case is where the converse prevails. For this first case, pore disappearance will prevail until the pores offer little hindrance to grain growth. The exact pore fraction this occurs cannot be predicted from the inclusion/grain growth data presented here, but observations reported by Kingery and Fransois[10] for UO_2 suggest that this phenomena can certainly occur when the pore volume fraction is ~ 0.10. In this case, the pores located at 4-grain junctions are dragged with the junction to maintain a uniform but magnified miocrostructure where the pore size to grain size ratio remains constant due to pore coalescence at newly formed 4-grain junctions.

The second extreme case, i.e., the case where the kinetics of pore disappearance is greater than grain growth kinetics, grain growth will be initially restricted to dense regions as discussed above. When the pore volume decreases to some critical volume fraction, the distribution of porosity will now govern the condition for grain growth as for the inclusion case. If this distribution is inhomogeneous, some dense regions will enlarge. Grain growth in these dense regions will result in much larger grains than in regions where grain growth is still hindered by porosity. This condition sets the stage for abnormal grain growth, i.e., grains within the dense regions rapidly grow to swallow neighboring grains and pores. Results presented for the ZrO_2 inclusions suggest that a inhomogeneous pore distribution can result in exaggerated grain growth for a volume fraction < 0.05.

Thus, it can be concluded that exaggerated grain growth is promoted by the nonuniform distribution of pores (or inclusions). Agglomerates that densify prior to the bulk are therefore prime candidates and sites for exaggerated grain growth.

ACKNOWLEDGEMENTS

This work was supported by the Air Force Office of Scientific Research, Contract F49620-81-C-0036. The authors greatly benefited from discussions with D.R. Green, P.E.D. Morgan and I. Aksay.

REFERENCES

1. F.F. Lange, "Fracture Mechanics and Microstructural Design," Fracture Mechanics of Ceramics Vol. 4, pp. 799-820, ed. by R.C. Bradt, D.P.H. Hasselman and F.F. Lange, Plenum Press (1978).

2. D.J. Green, ibid Vol. 6 (in press).

3. F.F. Lange and A. Arora, "Microcracking Phenomena and Strength of Al_2O_3/SiC Composites," to be published.

4. C. Zener, quoted by C.S. Smith, Trans. Met. Soc. AIME 175, 15 (1949).

5. M.F. Ashby and R.M.A. Centamore, "The Dragging of Small Oxide Particles by Migrating Grain Boundaries in Copper," Acta. Met. 16 1081 (1968).

6. P.G. Showman, "Movement of Small Inclusions in Solids by a Temperature Gradient," Trans. Met. Soc. AIME 230, 1134 (1964).

7. D.J. Green, "Critical Microstructures for Microcracking in Al_2O_3/ZrO_2 Composites," J. Am. Ceram. Soc. 65, 610 (1982).

8. C.H. Hsueh, A.G. Evans and R.C. Coble, "Microstructural Development During Final/Intermediate Stage Sintering - I. Pore/Grain Boundary Separation," Acta. Met. 30, 1269 (1982).

9. M.A. Spears and A.G. Evans, "ibid, II - Grain and Pore Coarsening," Acta. Met. 30, 1281 (1982).

10. W.D. Kingery and B. Francois, "Grain Growth in Porous Compacts," J. Am. Ceram. Soc. 48, 546 (1965).

END

DATE
FILMED

7-83

DTIC